



UNIVERSITATEA BABEȘ-BOLYAI  
BABEȘ-BOLYAI TUDOMÁNYEGYETEM  
BABEȘ-BOLYAI UNIVERSITÁT  
BABEȘ-BOLYAI UNIVERSITY  
TRADITIO ET EXCELLENTIA

Faculty of Chemistry and  
Chemical Engineering  
Babeș-Bolyai University,  
Cluj-Napoca  
Doctoral School of Chemical  
Engineering



**FARKAS NOÉMI- IZABELLA**

## **Advanced nanomaterials for biomedical applications**

*PhD Thesis*

*Summary*

**Scientific advisor:**

**Prof. Dr. Eng. Graziella – Liana TURDEAN**

**Cluj-Napoca**

**2024**

## Summary table of contents

<b>Summary table of contents</b> .....	2
<b>Thesis table of contents</b> .....	4
<b>Keywords</b> .....	7
<b>Introduction</b> .....	7
<b>I. Bibliographic Overview</b> .....	12
1. <i>Local drug delivery systems</i> .....	12
1.1. Study of the release mechanism.....	12
2. <i>Biomaterials for local drug delivery systems</i> .....	13
2.1. Bioceramics.....	14
2.2. Polymeric biomaterials .....	14
2.3. Metallic (implant) biomaterials.....	15
<b>II. Original contribution</b> .....	16
<b>Objectives of the thesis</b> .....	16
3. <i><math>\beta</math>-TCP, Si- and Mg-doped <math>\beta</math>-TCP synthesized by co-precipitation method for controlled drug delivery</i> .....	18
3.1. Experimental steps .....	18
3.2. Results and discussions.....	18
3.2.1. Optimization study .....	18
3.2.2. X-ray diffraction analysis .....	18
3.2.3. Morphological properties.....	19
3.2.4. Doxy adsorption study.....	20
3.2.5. Drug release study.....	21
3.2.6. Drug release mechanism.....	22
3.3. Partial conclusions.....	23
4. <i>The impact of hydroxyapatite-based biomaterials' chemical composition and morphology on their drug release characteristics</i> .....	24
4.1. Experimental part .....	24

4.2.	Results and discussions.....	24
4.2.1.	Particle size and morphological analysis .....	24
4.2.2.	Determination of Doxy content.....	25
4.2.3.	Doxy release from HA-based nanopowders .....	26
4.2.4.	Doxy release from HA-based microspheres .....	27
4.2.5.	Effect of release media on Doxy release .....	28
4.3.	Partial conclusions.....	30
5.	<i>Investigation of optimized poly(lactic acid)/hydroxyapatite/ doxycycline coatings on titanium alloy surfaces.....</i>	<i>31</i>
5.1.	Experimental steps .....	31
5.2.	Results and discussion .....	31
5.2.1.	Optimization study .....	31
5.2.2.	Morphological characterization of coatings .....	33
5.2.3.	In vitro corrosion behaviour.....	34
5.2.4.	Investigation of Doxy release .....	35
5.2.5.	Release kinetics study.....	36
5.3.	Partial conclusions.....	36
6.	<i>Real-time investigation of Doxycycline release by electrochemical method.....</i>	<i>38</i>
6.1.	Experimental steps .....	38
6.2.	Results and discussion .....	38
6.2.1.	Investigation of the electrochemical behaviour of Doxy.....	38
6.2.2.	Real-time release study of Doxy .....	39
6.2.3.	Validation of the DPV method .....	40
6.2.3.1.	Model-independent methodology.....	41
6.2.3.2.	Model-dependent methodology.....	42
6.3.	Partial conclusions.....	43
<b>III.</b>	<b>General conclusions.....</b>	<b>44</b>
	<b>References.....</b>	<b>52</b>

## Thesis table of contents

Preface.....	2
Table of contents.....	4
List of abbreviations and symbols.....	9
Introduction.....	11
I. Bibliographic Overview.....	16
1. <i>Oral pathology and orthopedic issues. Contemporary solutions and risks</i> .....	16
1.1. Structure of teeth and bones.....	16
1.2. Diseases and Treatments.....	16
2. <i>Drug delivery systems</i> .....	18
2.1. Local drug delivery systems in orthopedics and dentistry.....	19
2.2. Local antibiotic therapy.....	21
2.3. In vitro release study.....	23
2.4. Study of the release mechanism.....	25
3. <i>Biomaterials for local drug delivery systems</i> .....	29
3.1. Biomaterials.....	29
3.2. History of biomaterials.....	30
3.3. Classification of biomaterials.....	31
3.4. Bioceramics.....	32
3.4.1. Tricalcium phosphate.....	34
3.4.2. Hydroxyapatite.....	37
3.4.2.1. Drying techniques. Mini spray dryer.....	40
3.5. Polymeric biomaterials.....	41
3.5.1. Nanofibers. Electrospinning.....	42
3.5.2. Poly (lactic acid).....	44
3.5.3. PLA and PLA-based composite nanofibers.....	46
3.6. Metallic biomaterials.....	48
3.6.1. Implant materials.....	48
3.6.2. Surface modification, Dip-coating technique.....	50
3.6.3. Biocompatible and bioactive coatings.....	51
3.6.4. Combined use of metal implants and drug delivery systems.....	53
II. Original contribution.....	55
Objectives of the thesis.....	55
4. <i><math>\beta</math>-TCP, Si- and Mg-doped <math>\beta</math>-TCP synthesized by co-precipitation method for controlled drug delivery</i> .....	57
4.1. Experimental steps.....	57
4.1.1. Materials.....	57
4.1.2. Synthesis of $\beta$ -TCP and ion-doped $\beta$ -TCP.....	58
4.1.3. Physicochemical characterization.....	58
4.1.3.1. X-ray diffraction analysis.....	58
4.1.3.2. Morphological and chemical analysis.....	59
4.1.3.3. Analysis of particle size.....	59
4.1.3.4. Thermogravimetric and differential thermal analyses.....	59
4.1.4. Doxy adsorption study.....	59
4.1.5. Drug release study.....	60
4.1.6. Drug release mechanism.....	61
4.2. Results and discussions.....	61

4.2.1. Preliminary experiments.....	61
4.2.2. X-ray diffraction analysis.....	62
4.2.3. Thermal gravimetric and differential thermal analysis.....	65
4.2.4. Morphological and chemical properties of samples.....	67
4.2.5. Doxy adsorption study.....	71
4.2.6. Drug release study.....	72
4.2.7. Drug release mechanism.....	76
4.3. Partial conclusions.....	77
5. <i>The impact of hydroxyapatite-based biomaterials' chemical composition and morphology on their drug release characteristics</i> .....	79
5.1. Experimental part.....	79
5.1.1. Materials.....	79
5.1.2. Synthesis of HA.....	80
5.1.3. Synthesis of ion-doped HA.....	80
5.1.4. . Methods of drying precipitations.....	81
5.1.5. Carrier characterization.....	82
5.1.5.1. Particle size analysis.....	82
5.1.5.2. Scanning electron microscopy and Energy-dispersive X-ray spectroscopy analysis.....	82
5.1.5.3. Powder X-ray diffraction analysis.....	82
5.1.5.4. Thermal analysis.....	83
5.1.5.5. Determination of specific surface area (SSA) and porosity.....	83
5.1.6. The Doxy loading process.....	84
5.1.7. Measurement and characterization of release profiles.....	84
5.2. Results and discussions.....	85
5.2.1. Crystallographic analysis.....	85
5.2.2. Particle size and morphological analysis.....	87
5.2.3. The chemical composition of the samples.....	91
5.2.4. Thermal stability of the prepared samples.....	93
5.2.5. Determination of Doxy content.....	95
5.2.6. Determination of SSA and porosity.....	96
5.2.7. Measurement and characterization of release profiles.....	99
5.2.7.1. Doxy release from HA-based nanopowders.....	99
5.2.7.2. Doxy release from HA-based microspheres.....	102
5.2.7.3. Drug release studies.....	103
5.2.7.4. Effect of release media on Doxy release.....	105
5.2.7.5. Discussion of Doxy release profiles from different carriers.....	110
5.3. Partial conclusions.....	112
6. <i>Investigation of optimized poly(lactic acid)/hydroxyapatite/ doxycycline coatings on titanium alloy surfaces</i> .....	114
6.1. Materials and methods.....	114
6.1.1. Materials.....	114
6.1.2. Preparation of Ti64 specimens.....	115
6.1.3. Preparation of PLA and PLA/HA coating, for preliminary experiments.....	115
6.1.4. Preparation of polymer-based coating for experimental design.....	115
6.1.5. Experimental design.....	116
6.1.6. Preparation of drug-containing composite coatings.....	117
6.1.7. Characterisation of prepared coatings.....	118
6.1.7.1. Characterization of surface morphology and composition.....	118
6.1.7.2. Coating thickness.....	118

6.1.7.3.	Thermal stability.....	118
6.1.7.4.	Wettability analysis.....	119
6.1.8.	Investigation of corrosion behaviour in vitro.....	119
6.1.9.	Spectrophotometric investigation of drug release.....	119
6.1.10.	Drug release study.....	120
6.2.	Results and discussion.....	120
6.2.1.	Preliminary experiment.....	120
6.2.2.	Optimization study.....	123
6.2.3.	Morphological and elemental characterization of PLA, PLA_HA, PLA_D5, and PLA_HA_D5 coatings.....	134
6.2.4.	Thermogravimetric analysis.....	136
6.2.5.	Analysis of surface wettability.....	139
6.2.6.	In vitro corrosion behaviour.....	140
6.2.7.	Investigation of Doxy release.....	146
6.2.8.	Release kinetics study.....	147
6.3.	Partial conclusions.....	149
7.	<i>Real-time investigation of Doxycycline release by electrochemical method</i> .....	151
7.1.	Materials and methods.....	151
7.1.1.	Materials.....	151
7.1.2.	Preparation of Doxy nanofiber carriers.....	152
7.1.3.	Characterization of electrospun mats.....	152
7.1.3.1.	Scanning electron microscopy.....	152
7.1.3.2.	Fourier transform infrared spectroscopy.....	153
7.1.4.	Drug loading process.....	153
7.1.5.	In situ drug release study.....	153
7.1.6.	Drug release kinetics study.....	154
7.2.	Results and discussion.....	155
7.2.1.	Morphological discussion of nanofibers.....	155
7.2.2.	FT-IR spectroscopy analysis of nanofibrous carriers.....	156
7.2.3.	Loading of Doxy.....	158
7.2.4.	Investigation of the electrochemical behavior of Doxy.....	159
7.2.4.1.	Cyclic Voltammetry.....	160
7.2.4.2.	Influence of input signal parameters on DP voltammograms.....	161
7.2.5.	Doxy release study using an electrochemical method.....	162
7.2.5.1.	Determination of calibration curve.....	162
7.2.5.2.	Real-time release study of Doxy.....	163
7.2.6.	Validation of the DPV method.....	166
7.2.6.1.	Comparison of DPV drug release profiles with UV-VIS release profiles.....	166
7.2.6.2.	Model-independent methodology.....	167
7.2.6.3.	Model-dependent methodology.....	168
7.3.	Partial conclusions.....	171
III.	General conclusions.....	173
	Dissemination of results.....	181
	References.....	183

## Keywords

local drug delivery system; release kinetics; doxycycline; hydroxyapatite; polylactic acid; nanofibers; coatings; real-time monitoring

## Introduction

The tremendous progress in the field of drug delivery systems (DDSs) capable of delivering therapeutic agents into the body, in the last few decades has led to significant achievements, such as sustained - release drug administration or drug-loaded implantable devices. Additionally, the explosive emergence of nanotechnology has led to breath-taking results in medicine as well, making it possible to use new DDSs. Although the design of these DDSs requires a combination of technologies, due to nanomedicine, targeted drug delivery is now achievable.

Thanks to nano carrier-based DDSs, the revolutionization of drug administration can occur, as these systems, capable of overcoming physical and biological barriers, can provide controlled and prolonged drug release. One group of DDSs is *local drug delivery systems* (LDDSs). Their effectiveness lies in significantly enhancing the therapeutic effect of the active substance at the target site, thus minimizing potential side effects caused by the active molecule.

The use of LDDSs has proven globally beneficial in orthopedics and dentistry as well. Their application is justified and necessary because although the implants are biocompatible and most of them bioactive, only a few of these materials have antimicrobial properties. LDDSs can offer solutions for the treatment of inflammatory or infection-prone sites and even for preventing the development of infections. The local application of antibiotic therapy also minimizes the development of further diseases. Improving the therapeutic index and the joint development of drug-biomaterial carriers significantly reduces the risk of implant rejection and can provide a solution for long-term treatments.

However, many advances and developments are still the results of basic research. The actual implementation of potentially applicable systems in various fields of medicine can represent a huge-scale development. However, there are still numerous gaps that need to be addressed. Despite numerous studies reporting the beneficial use of local antibiotic therapy, standardization has not yet been achieved. Due to these drawbacks and shortcomings, there is still no clear DDS. The issue of customization further complicates the design problem. In the case of the majority of LDDSs, the complete therapeutic mechanism required for their application is still unknown, and even for specific devices, research reflects divisive opinions

and results. These include issues of biocompatibility, safety, stability, and controllability. Beyond scientific limitations, resolving scalability and technological barriers also requires further development.

The present doctoral thesis *aims* to enhance the effectiveness of treating hard tissue diseases through the research and development of LDDSs that enable targeted and efficient therapy.

The main inorganic component of bones and teeth is hydroxyapatite (HA), a bio-material that can be easily produced synthetically. Its medical application is made possible by its similarity to biological apatite due to its similar chemical structure. Often referred to as the “gold standard” of bio-materials, HA has long been known to accelerate healing processes in hard tissue implantation, in addition to being biocompatible, is also bioactive. Today's research goes beyond physical, mechanical, and biological analyses. Current development trends focus on investigating HA as an active substance carrier in medicine. The results presented below are mainly focused on the application of HA as LDDS, in three different systems: in bone substitute powder form, in polymer-composite film form, and in polymer nanofibers.

However, in addition to HA, other calcium phosphates are also suitable for bone replacement. An example of this is the bioresorbable  $\beta$ -tricalcium phosphate ( $\beta$ -TCP), which due to its excellent biological properties, can also be used in tissue engineering. Upon entering the body, the release of calcium and phosphate ions leads to the formation of bone-like apatite, balancing the processes of bone formation and attachment to pre-existing hard tissue.

Although the biological properties of these calcium phosphates (CaPs) are undisputed, their applicability is hindered by their weak physical and mechanical properties. Certain procedures, such as composite formation with polymers or ion substitution, can significantly improve these properties and open up numerous new possibilities for applications. Ion substitution has several other advantages as well, as the incorporation of silver or zinc into the structure results in antibacterial effects of the biomaterial. Silicon- and magnesium-substituted HA and  $\beta$ -TCP play a crucial role in physiological processes, primarily facilitating regeneration processes.

As can be seen from this summary, the doctoral thesis was divided into two main parts. The *Bibliographic overview* provides a comprehensive description of local drug carrier systems and biomaterials suitable as drug carriers (bioceramics, biopolymers, metallic biomaterials). Following a thorough literature review, the *Original contribution* section outlines the objectives and aims of the four chapters. The presentation of the experimental parts follows a

similar structure, including the materials and methods section (experimental steps), results and discussions, and conclusions.

Following current research trends, the first two chapters of the original contribution of the thesis focus on studying the drug-delivery capabilities of the previously mentioned CaPs. The studies used doxycycline (Doxy) as the test drug, which in addition to being a broad-spectrum antibiotic, shows a high affinity towards various CaPs. In the fourth chapter, entitled **“ $\beta$ -TCP, Si- and Mg-doped  $\beta$ -TCP synthesized by co-precipitation method for controlled drug delivery”**, the release of Doxy was investigated from the carriers mentioned in the title. Nevertheless, this study includes the empirical optimization of  $\beta$ -TCP synthesis by co-precipitation method, characterization of the synthesized carriers, drug loading, and drug release studies.

In general, the co-precipitation method allows for the production of various CaP morphologies, including the formation of porous aggregate structures. Structural porosity serves not only as active sites for bone formation processes, but also results in reduced drug release. Diffusion of drug molecules trapped in the pores is hindered, facilitating long-term release. The presence of foreign ions also favors the retard effect, which results in slower diffusion of the active substance. Furthermore, the amount of released drug can be controlled by the initial drug content. By increasing the initial active substance content, a significant decrease in dissolution rate can be achieved.

In the fifth chapter of the thesis (**“The impact of hydroxyapatite-based biomaterials' chemical composition and morphology on their drug release characteristics”**), the release mechanism of Doxy from HA produced by the co-precipitation method and ion-doped HA was examined. Essentially, this is a comparative study that discusses factors influencing drug release, such as the chemical composition and morphology of HA powder and the importance of the dissolution medium in *in vitro* processes. The majority of the samples involved in the comparison are diffusion-controlled systems providing regular Doxy release.

Achieving controlled drug release depends on careful selection design and process parameters. Design processes take into account the main release mechanisms, so the system to be developed can be pre-regulated. Analyzing the experimental release profiles, and determining and characterizing drug transport mechanisms helps in understanding the release mechanism, discussing the extent of influencing parameters, and shaping the system according to therapeutic requirements.

The complex environment of the human body and the local limitations of the therapeutic site often demand the use of more intricate LDDSs, which require the design and development of various morphologies. Thus, moving forward in our research, was implemented HA (with regular microsphere morphology) containing Doxy for actual implant coatings. The sixth chapter of the experimental section (Original contribution) of the thesis is based on the combination of implant materials and LDDSs. Functionalization of the implant surface with LDDSs can result in a drastic reduction in post-operative complications. The primary objective of these devices is to prevent infections. The active substance can be properly applied to the surface of the implant using some biocompatible polymer. The most important role of HA in the surface functionalization of the implant is to improve biocompatibility and promote physiological processes.

In the presented research, the coatings produced by the dip-coating method are based on polylactic acid (PLA). PLA is a biodegradable and biocompatible polymer with significant medical importance. It is used in various medical fields, including tissue engineering. It is suitable for the delivery of active molecules, and the specific properties of the polymer have a significant impact on the release.

In the chapter entitled “**Investigation of optimized poly(lactic acid)/hydroxyapatite/doxycycline coatings on titanium alloy surfaces**”, we also looked for answers to questions such as factors influencing the porosity of polymer coatings. Porosity plays a crucial role not only in bioactivity, but also in drug release mechanisms and corrosion resistance. The experimental design, including the Box-Behnken response surface method, is suitable for optimizing the pore size and thickness of the coatings, examining the effect of the experimental parameters, and significantly reducing the number of experiments to be performed. The success of the design lies in its efficiency compared to other similar response surface methodologies.

The experimental parameters enable the production of porous Doxy-loaded PLA and PLA/HA coatings. The additives change the characteristics of the PLA coating, its wettability, and thus its corrosion resistance also changes. Drug transport can be controlled by the chemical and physical properties of the coating. Therefore, due to the diverse nature of the biomaterials composing the complex coating, it becomes possible to achieve multi-stage drug release as recommended by local antibiotic therapy.

Taking advantage of new trends and opportunities in the design of LDDS, the drug carrier properties of HA were investigated in a novel morphological approach, namely in nanofibers produced by electrospinning. Nanofibers, owing to their texture, are not as suitable for bone implants but rather for applications in dental interventions, such as incorporation into the

periodontal pocket. However, numerous medical applications are also known, for example, targeted active material delivery, tissue engineering, or wound dressing.

The use of nanofibers as drug carriers is increasingly becoming the focus of research. The drug-binding process is crucial for drug release. There are several methods for the preparation of the drug-loaded nanofiber: the drug can be encapsulated within the fibers during the fiber formation process (electrospinning process), or it can be bound to the surface of the fibers during post-electrospinning processes. In the latter case, the sequential release is easily achieved, since in the first step the molecules of the weakly bound active ingredient diffuse. The properties of the polymer can control the following stages.

In the chapter “**Real-time investigation of Doxycycline release by electrochemical method**”, the goal was to investigate drug release from Doxy-loaded nanofibers bound by physical adsorption. This research part focused on innovating the *in vitro* monitoring of drug release.

Performing and repeating *in vitro* experiments are essential in the design and development of LDDSs. However, the dissolution kinetics is not only influenced by the parameters discussed in the thesis, but also by the measurement method. For instance, dilution processes associated with continuous sampling, while simulating the flow of fluids in the body, may affect the release mechanism. Conventional UV-VIS spectroscopy or HPLC measurement methods are intermittent, so sampling is essential. Among electrochemical methods, particularly voltammetric techniques, some can be applied with sufficient precision and sensitivity for *in situ* measurement of drug release. One such method is the Differential Pulse Voltammetry (DPV). Compared to traditional methods, DPV is a cheaper and simpler procedure, allowing for faster measurements without the interference of any external factors.

The final part of the thesis included the *general conclusions* of the thesis, the *valorization of the results* achieved during the doctoral studies and the *bibliographic references* used for sustaining and explaining the obtained experimental results.

## **I. Bibliographic Overview**

### **1. Local drug delivery systems**

Drug delivery systems (DDS) can be defined most simply as devices that are suitable for the targeted introduction of one or more therapeutic agents into the human body [1-2]. The possibilities offered by nanotechnology are promising, especially biomaterial-drug systems, which are of outstanding importance. Due to their unique properties, they offer a new and beneficial opportunity in clinical practice [3].

The use of biomaterials as local drug carriers is becoming increasingly common in many fields of medicine, including dentistry and orthopedics. Although there are many gaps in this area [4], the LDDS allows the drug release directly at the therapeutic site [5]. The use of LDDS is possible in several dental areas, such as oral diseases [6-7], anesthesiology [8], restorative dentistry [9], periodontics and endodontic [10], prosthodontics [11] and implantology [12]. The use of LDDSs at the target site significantly increases the efficacy of the drug [13]. The regulated drug release is an important advantage, as the design allows control of the target site, release period, and release rate [14]. Research reports has shown that the use of this type of system reduces recovery time [15] and improves osseointegration [16].

#### **1.1. Study of the release mechanism**

During the design and development of LDDSs, special attention was paid to systems providing controlled drug release. Diffusion plays a crucial role in the majority of controlled and regulated DDS [17-19]. The phenomenon of diffusion is usually defined as a mass transfer process in which the driving force is the concentration gradient. The diffusion is of crucial importance in the pharmaceutical and medical fields, since in addition to controlling drug release, it is also responsible for the absorption of the active ingredient in the targeted tissue or cell [20].

Continuously developing science and interdisciplinarity have made it possible to predict the release profile of a given DDS by performing different calculation algorithms. Mathematical models and experimental observations permit *in vitro* and *in vivo* drug release analysis, their correct combined use helps to understand the release mechanism, thereby providing answers to questions related to drug release.

Several methods can be used to study drug release kinetics, which can be divided into three categories: statistical methods, model-dependent, and model-independent methods. In order to understand the drug release kinetics and to predict further behavior, it is necessary to

use model-dependent approaches. These are mathematical functions that describe the release of the given drug from the DDS. **Table 2** presents the main kinetic models, their associated equations, and the most important characteristics [21].

**Table 2:** The most commonly used mathematical models describing drug release kinetics.

Kinetic model	Mathematical equation	S.N.	The main features of the model
<b>Zero order</b>	$Q_t = Q_0 - k_0 * t$	(3)	<ul style="list-style-type: none"> <li>○ The release is independent of the initial drug concentration;               <ul style="list-style-type: none"> <li>○ Constant release</li> </ul> </li> </ul>
<b>First-order</b>	$\log Q_t = \log Q_0 + \frac{k_1 * t}{2.303}$	(4)	<ul style="list-style-type: none"> <li>○ The release is dependent of the initial drug concentration;               <ul style="list-style-type: none"> <li>○ Sustained release</li> </ul> </li> </ul>
<b>Higuchi</b>	$Q_t = k_H * t$	(5)	<ul style="list-style-type: none"> <li>○ Release according to Fick-diffusion;</li> <li>○ Linearly proportional to the square root of time</li> </ul>
<b>Hixson-Crowell</b>	$Q_0^{1/3} - Q_t^{1/3} = k_{HC} * t$	(6)	<ul style="list-style-type: none"> <li>○ Dissolution controlled release;</li> <li>○ Surface changes of drug delivery, particles size decrease over time</li> </ul>
<b>Korsmeyer-Peppas</b>	$\frac{Q_t}{Q_\infty} = k_{KP} * t^n$	(7)	<ul style="list-style-type: none"> <li>○ The value of the diffusion coefficient n determines the mechanism of release of the active ingredient               <ul style="list-style-type: none"> <li>• <math>n &lt; 0.5</math>: quasi fickian diffusion</li> <li>• <math>n = 0.5</math>: fickian diffusion</li> <li>• <math>0.5 &lt; n &lt; 1</math>: anomalous diffusion                   <ul style="list-style-type: none"> <li>• <math>n = 1</math>: case II transport</li> <li>• <math>n &gt; 1</math>: super case II transport</li> </ul> </li> </ul> </li> </ul>

where:  $Q_t$  is the amount of drug released at time  $t$ ;  $Q_0$  is the initial amount of drug;  $Q_\infty$  is the amount of drug released at the time  $\infty$ ;  $k_0$ ,  $k_1$ ,  $k_H$ ,  $k_{HC}$ , and  $k_{KP}$  are the zero-order, first-order, Higuchi's, Hixson's and Korsmeyer-Peppas release rate constant, respectively;  $n$  is the diffusional release exponent

In the case of Korsmeyer-Peppas model, the limit of the diffusion exponent ( $n$ ) can vary based on the sample geometry. Accordingly, for a thin film,  $n = 0.5$ , for a sphere,  $n = 0.45$ , and for a cylindrical particle,  $n = 0.43$  [22].

## 2. Biomaterials for local drug delivery systems

Biomaterials include all substances or combinations of materials that can be incorporated into the human body and whose effect improves or maintains the quality of life. So, their

application can have two main purposes: diagnostic and/ or therapeutic [23]. These are usually devices that supplement or replace some kind of tissues, from the category of both natural and synthetic materials. When biomaterials are implanted in the body, they interact with it, and their biocompatibility determines the response [24].

## 2.1. Bioceramics

Bioceramics, or ceramic-based biomaterials, consist of molecules in which metallic or non-metallic elements are bounded by covalent or ionic bonds. Of course, it is possible for both bond types to be found in the same molecule [25]. The largest and most significant group of materials belonging to bioceramics are calcium phosphates (CaPs). CaPs are able to integrate into the physiological environment within a short time and with minimal risk [26].

**Tricalcium phosphate** (TCP) is one of the most important compounds of bioresorbable CaPs. Its general formula is  $\text{Ca}_3(\text{PO}_4)_2$ , the Ca/P ratio is 1.5 and its molecular weight is 310.17 g/mol. From a crystallographic point of view,  $\beta$ -TCP belongs to rhombohedral crystals with space group R3c. Its specific biological properties make it suitable for use in tissue engineering, both for bones and teeth treatment [27].

**Hydroxyapatite** is the real 'gold standard' of biomaterials, as it is used in both orthopedic and dental applications. Its general formula is  $\text{Ca}_5(\text{PO}_4)_3(\text{OH})$ , in which the Ca/P ratio for stoichiometric HA is 1.67, while for non-stoichiometric HA it is between 1.5 and 1.67 [28], with molecular weight of 502.31g/mol. HA is the main inorganic component of bones, teeth and tooth enamel. In this way, synthetic HA is easily recognized and accepted by the body. It has excellent biological properties, as it is bioactive, biocompatible, osteoinductive, osteoconductive and osteointegrative [29]. HA is suitable for bone scaffold, implant coating and for delivery active molecules [29-31]. The surface of the HA promotes the interaction between the carrier and the active molecules [32], and between the carrier and the cells [33].

## 2.2. Polymeric biomaterials

Another important group of biomaterials and the group of compounds that are suitable for drug delivery are polymers. Polymers are macromolecules built by covalently bonded monomers [34]. Polymers are the most widely used material, both in science and everyday life [35]. They also have an outstanding role as DDSs [36], for example in the form of films and coatings [37-38], and microfibers and nanofibers [39-40].

According to the traditional definition, **polymer nanofibers** are cylindrical structures with a diameter of up to a few 100 nm and an aspect ratio greater than 50 [41]. The

electrospinning process proves to be the most suitable for the production of continuous nanofibers, most of the methods are only suitable for the production of discontinuous fibers.

The **poly(lactic acid)** (PLA) is a biocompatible, non-toxic, non-carcinogenic compound, and its degradation products are also non-toxic [42-43]. The use of PLA in therapeutic treatments was already approved by the FDA in 1970 [44]. Nowadays, it can be used in cancer therapy, regenerative medicine, wound management, tissue engineering, stent applications, dental and orthopedic fields, and also as a drug carrier [43-45]. PLA has proven to be suitable for delivering small drug molecules [46] as well as large proteins and nucleic acids [47].

### **2.3. Metallic (implant) biomaterials**

In hard tissue implantology, Ti and Ti - alloys are most commonly used [48-49], followed by 316L stainless steel [50] and cobalt-based alloy [51-52]. Ti and Ti-based alloys receive significant attention in both the medical and material science fields. Its main application is complete bone and/or tooth replacement. Among the Ti alloys, implants made of the Ti-6Al-4V (Ti64) alloy satisfy more than 50% of the needs [53]. This bioinert alloy has significantly higher rigidity than natural bone [54]. Its advantageous properties compared to other, also frequently used metallic alloys, is its relatively low density ( $4.5 \text{ g/cm}^3$ ), and low elastic modulus (110 GPa) [55].

Surface modification or even surface functionalization results in implants with improved biological and mechanical properties [56-57]. Clinical efficiency can be achieved by increasing the biocompatibility and bioactivity of the surfaces, which promote osseointegration and enhance the development of interactions between the implant and the surrounding tissues. Homogeneity, uniform thickness, and porosity are crucial criteria for the suitability of coatings. The three-step dip-coating technique is suitable for the production of large quantities of coatings with controlled porosity and film thickness.

Thanks to developing science, the combination of metal implants with DDSs is possible, so they have a local drug-delivery role. The combinatorial therapy proves to be a more beneficial form of treatment. The active substance is not applied directly to the implant surface, some type of carrier matrix is required to obtain the appropriate system [9]. On the one hand, the carrier matrix has a transport and protective role in order to successfully deliver the active molecule to its target site, and on the other hand, it must meet the expected properties typical of coatings [58].

## II. Original contribution

### Objectives of the thesis

The research of this doctoral thesis *aims* to contribute to the study, development, and optimization of local drug-delivery systems that increase the efficacy of the treatment of hard tissue diseases. Within the LDDS, the emphasis of the thesis is on local antibiotic therapy, with the investigation of systems using Doxycycline (a broad-spectrum antibiotic). *The central goal* is to develop and produce systems that ensure prolonged drug release. Another key goal is to achieve the appropriate release mechanism through a thorough investigation of factors influencing the Doxy release.

The aim is to investigate CaPs, primarily as drug carrier systems. The justification of the topic was supported by a thorough review of the literature, since, although there are numerous studies on the subject, there are gaps in the issues of local drug carriers. The main goal of the doctoral thesis is to investigate and understand the drug release mechanism, considering aspects such as the chemical structure and morphology of the carrier, or the effect of the initial drug content of the system. Additionally, the aim was to study the *in vitro* drug release not only from bone substitute powders but also from polymer nanofibers and polymer composite films. Special attention was paid to the effect of HA on the properties of these systems.

Based on these presented goals, the doctoral thesis was divided into *four chapters*, the individual objectives of which are described below.

#### **1. $\beta$ -TCP, Si- and Mg-doped $\beta$ -TCP synthesized by co-precipitation method for controlled drug delivery**

- Optimization of co-precipitation reaction for the synthesis of pure  $\beta$ -TCP and  $\beta$ -TCP doped with biologically active ions ( $\text{Mg}^{2+}$  or  $\text{SiO}_4^{4-}$ )
- Characterization of the carriers using conventional material characterization methods
- Examination of  $\beta$ -TCP powders as LDDSs under *in vitro* conditions

#### **2. The impact of hydroxyapatite-based biomaterials' chemical composition and morphology on their drug release characteristics**

- Preparation of HA, Si-doped HA and Mg-doped HA, which ensures the sustained release of Doxy, by the co-precipitation method and the characterization of the powders, as well as the investigation of the effect of the Si source (used in the synthesis) on the properties of the carrier

- Production of various morphologies of HA powders through different drying techniques (conventional drying and spray dryer method) and comparison of these powders in terms of local drug carriers
- Detailed investigation of factors influencing the release of Doxy (chemical composition, morphology, release medium), as well as demonstrating the effect of initial active substance amount, also in the case of HA-based powders

### **3. Investigation of optimized poly(lactic acid)/hydroxyapatite/ doxycycline coatings on titanium alloy surfaces**

- Production of Doxy-containing, porous PLA and PLA-HA coatings using a simple dip-coating method
- Optimizing the porosity and thickness of coatings in order to achieve controlled and prolonged Doxy release
- Characterization of coatings and investigation of their anti-corrosion properties, using electrochemical method

### **4. Real-time investigation of Doxycycline release by electrochemical method**

- Preparation of PLA and HA-containing PLA nanofibers by the electrospinning method, and binding of the active substance (Doxy) on the electrospun mats by a post-electrospinning method
- Innovating the measurement of Doxy release under *in vitro* conditions, in situ real-time monitoring of drug release, without sampling, utilizing the differential-pulse voltammetry method.
- Verification of the electrochemical method using UV-VIS spectroscopic measurements and validation of the results using model-dependent and model-independent approaches

### **3. $\beta$ -TCP, Si- and Mg-doped $\beta$ -TCP synthesized by co-precipitation method for controlled drug delivery**

#### **3.1. Experimental steps**

Based on the current literature, the drug delivery properties of tricalcium phosphates are less explored. Therefore, it was justified that the first part of the doctoral thesis aimed to investigate pure  $\beta$ -TCP as well as  $\text{SiO}_4^{4-}$ - and  $\text{Mg}^{2+}$ -substituted  $\beta$ -TCP as drug delivery systems. Ions that are currently the focus of bone regeneration research were used for ion doping. The experiments were performed with a broad-spectrum antibiotic, doxycycline.

Pure  $\beta$ -TCP powder and different ion-doped  $\beta$ -TCP were synthesized by a simple and controllable co-precipitation method followed by heat treatment. The characterization of the prepared samples was investigated using X-ray diffractometry (XRD), thermal analysis (TG), scanning electron microscopy (SEM), energy-dispersive X-ray analysis (EDX), and particle size analyzer (PSA). The Doxy adsorption and release study was measured spectrophotometrically.

#### **3.2. Results and discussions**

##### **3.2.1. Optimization study**

The co-precipitation method was empirically optimized to produce high-purity  $\beta$ -TCP. Thermal analysis and XRD analysis were used to evaluate the reaction, and to analyse the phase purity and crystallinity of the samples. Mixing the reaction mixture for 2 hours (at pH=8) and then heat-treating the precipitate at 900 °C resulted in the formation of phase-pure  $\beta$ -TCP. Ion-doped  $\beta$ -TCPs were synthesized under these conditions.

##### **3.2.2. X-ray diffraction analysis**

The results of the XRD analyses of the ion-substituted samples are presented in **Figure 10**. It is evident from the plot that both the Si- and Mg-doped samples exhibit diffraction peaks that closely match the data for standard  $\beta$ -TCP.

The ion substitution resulted in a shift of characteristic peaks [59]. The crystallographic changes induced by cationic ion substitution were much more significant than in case of Si-doping, where only some differences in intensity changes were observed. When comparing the diffractograms of pure  $\beta$ -TCP and  $\beta$ -TCPMg, a noticeable shift of diffraction peaks towards higher values was observed. Accordingly, the characteristic peaks identified at 46.91° and 52.95° were shifted to values of 2 $\theta$ , 47.42° and 53.4°, respectively [60]. The successful incorporation of Mg into the structure was also indicated by the decrease in the degree of

crystallinity compared to pure  $\beta$ -TCP. The presence of Mg ions hindered crystallization, as observed by others [61], while silicon promoted crystallization processes.

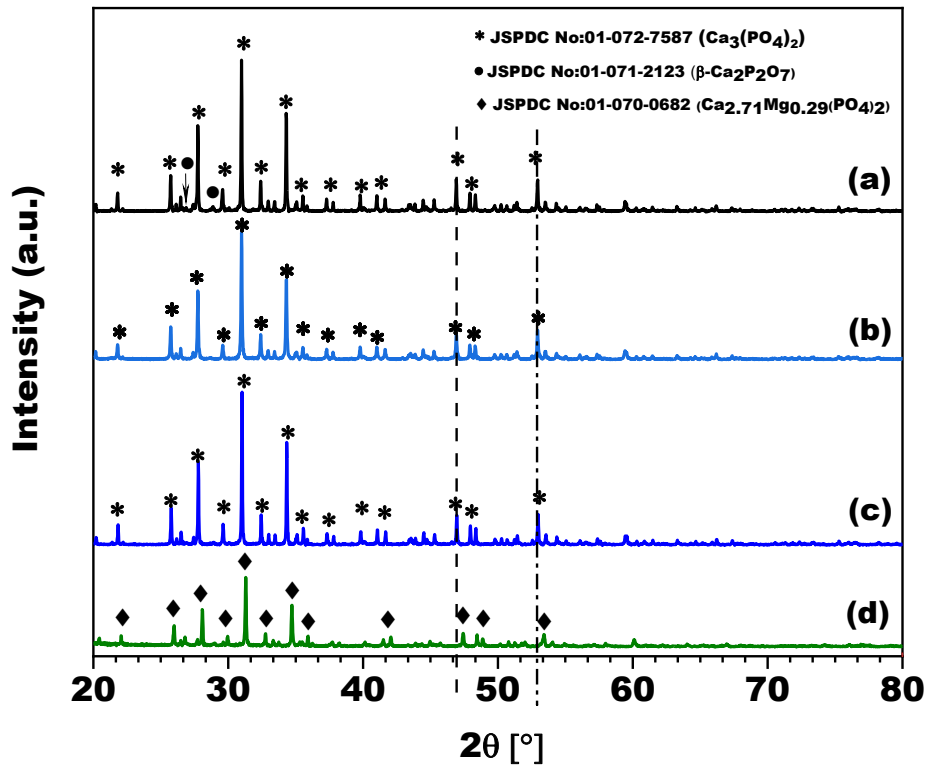


Figure 10: XRD diffractograms of (a)  $\beta$ -TCP, (b)  $\beta$ -TCPSi(1), (c)  $\beta$ -TCPSi(2), and (d)  $\beta$ -TCPMg, respectively

### 3.2.3. Morphological properties

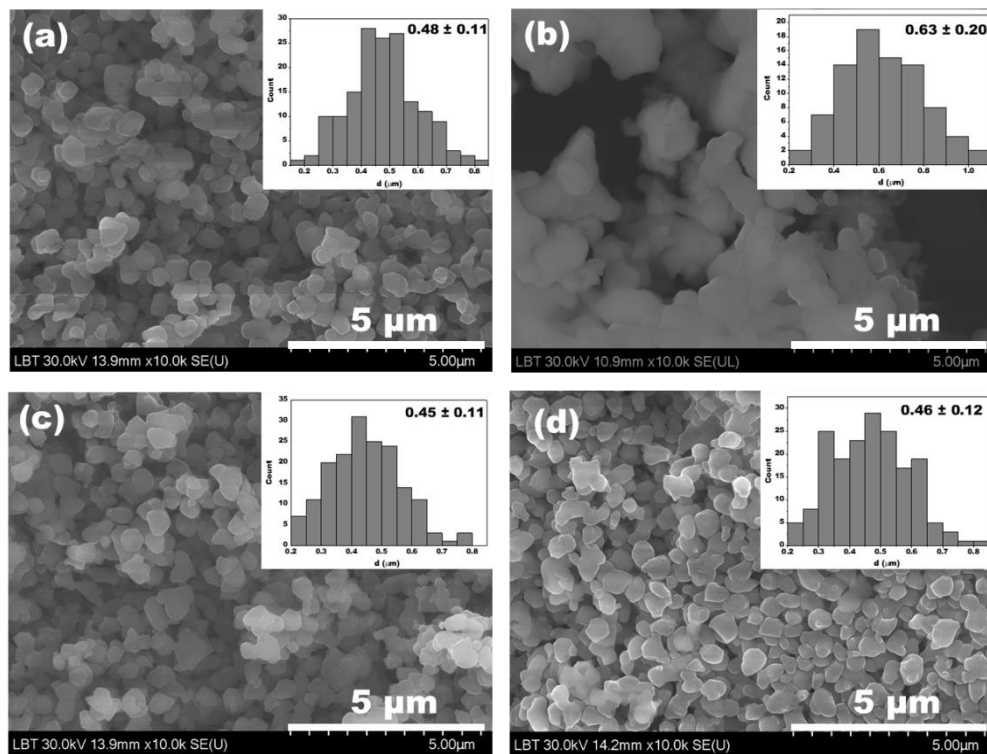
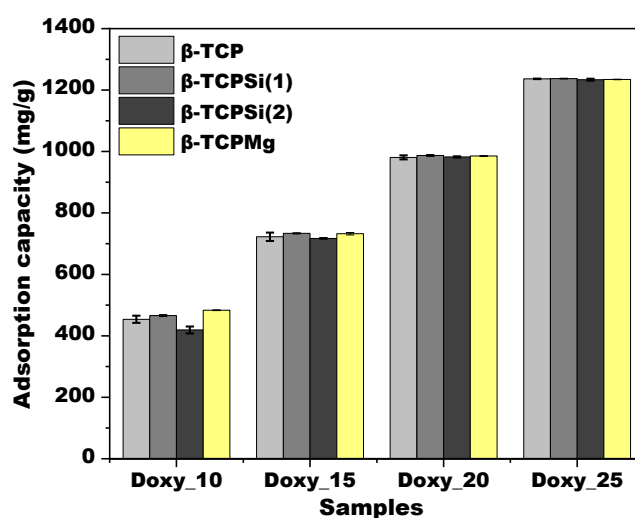


Figure 12: Morphology of (a) pure  $\beta$ -TCP, (b)  $\beta$ -TCPMg, (c)  $\beta$ -TCPSi(1), (d)  $\beta$ -TCPSi(2) samples and the corresponding histograms presenting the particle size distribution (inset)

The morphologies of the  $\beta$ -TCP,  $\beta$ -TCPMg,  $\beta$ -TCPSi(1), and  $\beta$ -TCPSi(2), prepared at 900 °C were presented in **Figure 12**. The  $\beta$ -TCP particles were predominantly uniform, spherical (or circular) in shape. The particle size distribution fell into a narrow range, with an average particle size of 480 nm. No significant changes were observed due to the Si substitution, the morphology of the particles was quite similar, regardless of the Si source used during the synthesis. The presence of Si, compared to pure  $\beta$ -TCP, resulted in a slight decrease in particle size (450 and 460 nm for  $\beta$ -TCPSi(1) and  $\beta$ -TCPSi(2), respectively) [62]. In addition, the tendency of the particles to aggregate was observed. Porous aggregates were most prominent in the case of  $\beta$ -TCPMg, where the average particle size was also larger, 630 nm.

The nano-size of the powders was verified using a PSA. The individual particles formed larger aggregates and were not present as individual particles in the bulk material. The average particle size of the powders was between 0.635 and 0.887  $\mu$ m. This real particle size is more decisive for the drug loading perspective than the size of individual particles [63].

### 3.2.4. Doxy adsorption study



**Figure 15:** The adsorption capacity (mg/g) of (a) pure  $\beta$ -TCP, (b)  $\beta$ -TCPMg, (c)  $\beta$ -TCPSi(1), (d)  $\beta$ -TCPSi(2) powders at different initial Doxy concentrations

High adsorption capacity values were achieved for each sample, ranging from 419 mg/g ( $\beta$ -TCPSi(2)\_Doxy\_10) to 1237 mg/g ( $\beta$ -TCPSi(1)\_Doxy\_25). This high affinity between Doxy molecules and  $\beta$ -TCP, as well as ion-doped  $\beta$ -TCP, is a promising property from the point of view of drug delivery. Regardless of the presence or absence of the foreign ion, a clear increasing tendency of the amount of active substance bound on the carrier with the initial drug concentration was observed. As can be seen in **Figure 15**, the effect of the concentration of the Doxy solution used for adsorption was highly significant. By increasing the concentration from

10 g/L to 25 g/L, a nearly threefold increase in drug loading was observed. The key role of drug concentration in drug loading via physical adsorption has been reported by other researchers [64-65].

### 3.2.5. Drug release study

The release profiles of drug-loaded samples were compared according to two aspects. Firstly, the effect of initial drug content for the same carrier was investigated, and secondly, the differences in release profiles were discussed based on the chemical composition of the carriers. The release profiles of Doxy (**Figure 16**) showed a similar increasing trend, regardless of the chemical composition of the investigated systems. In most samples with low initial Doxy content, a two-stage release was observed: an initial burst release followed by a slower, sustained release. This burst release was attributed to the rapid and intense diffusion of weakly bound active molecules on the surface of the carrier [66].

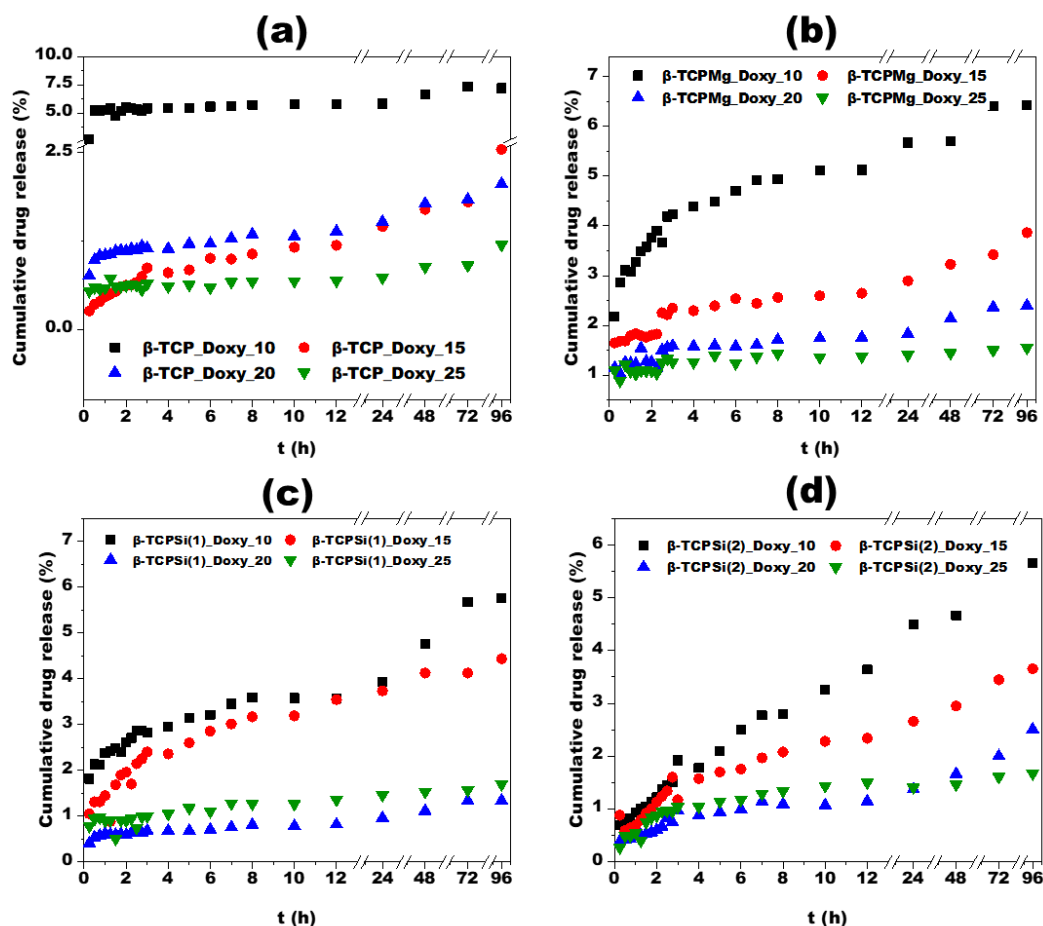


**Figure 16:** Cumulative Doxy release profile from (a)  $\beta$ -TCP-, (b)  $\beta$ -TCPMg-, (c)  $\beta$ -TCPSi(1)-, and (d)  $\beta$ -TCPSi(2)- based systems

Increasing the Doxy content in different  $\beta$ -TCPs resulted in a decrease in the released drug quantity, for example, 7.5% for  $\beta$ -TCP\_Doxy\_10 and 1.25% for  $\beta$ -TCP\_Doxy\_25. This trend was observed for all carriers. The possible reason for this is the interactions between drug molecules. The Doxy-Doxy interaction was probably stronger, so the rapid release from the surface was also hindered, not only from the pores.

In the case of samples with a small initial Doxy content, a retard effect was remarked. Comparing the  $\beta$ -TCP\_Doxy\_10,  $\beta$ -TCPSi(1)\_Doxy\_10,  $\beta$ -TCPSi(2)\_Doxy\_10, and  $\beta$ -TCPMg\_Doxy\_10 samples, the highest amount of active substance released was measured for the pure  $\beta$ -TCP carrier. Compared to pure CaPs, Si-containing CaPs are able to form stronger secondary interactions with the active substances [67-68]. The Si-OH groups resulted in a retard effect on the carrier, which means that the drug release was hindered due to stronger interactions. Thus, fewer drug was released over time [69].

### 3.2.6. Drug release mechanism

**Table 5:** *In vitro* drug release kinetics studies of investigated samples

<i>Samples</i>	<i>Zero-order</i>	<i>First-order</i>	<i>Hixson-Crowell</i>	<i>Higuchi</i>		<i>Korsmeyer-Peppas</i>		
	R <sup>2</sup>	R <sup>2</sup>	R <sup>2</sup>	R <sup>2</sup>	k <sub>H</sub>	R <sup>2</sup>	k <sub>KP</sub>	n
<i><math>\beta</math>-TCP_Doxy_10</i>	0.554	0.564	0.561	0.651	0.284	0.620	4.769	0.094
<i><math>\beta</math>-TCP_Doxy_15</i>	0.841	0.843	0.842	0.945	0.211	<b>0.976</b>	2.09	0.357
<i><math>\beta</math>-TCP_Doxy_20</i>	0.855	0.856	0.856	<b>0.959</b>	0.116	0.957	1.005	0.139
<i><math>\beta</math>-TCP_Doxy_25</i>	0.910	0.867	0.911	<b>0.911</b>	0.054	0.707	1.729	0.098
<i><math>\beta</math>-TCPMg_Doxy_10</i>	0.594	0.600	0.598	0.793	0.402	<b>0.941</b>	3.263	0.171
<i><math>\beta</math>-TCPMg_Doxy_15</i>	0.767	0.771	0.770	0.905	0.230	<b>0.933</b>	1.812	0.154
<i><math>\beta</math>-TCPMg_Doxy_20</i>	0.743	0.746	0.745	0.876	0.138	<b>0.886</b>	1.255	0.138
<i><math>\beta</math>-TCPMg_Doxy_25</i>	0.436	0.437	0.435	0.599	0.054	<b>0.806</b>	1.029	0.080
<i><math>\beta</math>-TCPSi(1)_Doxy_10</i>	0.846	0.851	0.849	0.961	0.410	<b>0.983</b>	2.314	0.192
<i><math>\beta</math>-TCPSi(1)_Doxy_15</i>	0.583	0.587	0.586	0.785	0.370	<b>0.860</b>	1.532	0.274
<i><math>\beta</math>-TCPSi(1)_Doxy_20</i>	0.884	0.885	0.885	<b>0.974</b>	0.094	0.953	1.812	0.179
<i><math>\beta</math>-TCPSi(1)_Doxy_25</i>	0.609	0.611	0.611	<b>0.761</b>	0.102	0.673	1.168	0.148
<i><math>\beta</math>-TCPSi(2)_Doxy_10</i>	0.756	0.762	0.760	0.919	0.609	<b>0.958</b>	1.028	0.422
<i><math>\beta</math>-TCPSi(2)_Doxy_15</i>	0.731	0.735	0.734	0.895	0.336	<b>0.899</b>	1.099	0.331
<i><math>\beta</math>-TCPSi(2)_Doxy_20</i>	0.862	0.864	0.864	0.952	0.208	<b>0.958</b>	1.888	0.324
<i><math>\beta</math>-TCPSi(2)_Doxy_25</i>	0.433	0.435	0.434	0.639	0.130	<b>0.792</b>	1.600	0.281

The precise understanding of drug release kinetics, mechanism, and thereby the controllability of release rate is crucial in the development of DDSs. Different models were applied to the obtained Doxy release data, and the most fitting models were selected and discussed. **Table 5** represents the determination coefficients of the examined models and the release constants for Higuchi and Korsmeyer-Peppas models.

The graphic representation of the amount of released Doxy from the  $\beta$ -TCP\_Doxy\_20,  $\beta$ -TCP\_Doxy\_25,  $\beta$ -TCPSi(1)\_Doxy\_20, and  $\beta$ -TCPSi(1)\_Doxy\_25 systems against the square root of time showed a close linear relationship, suggesting that the release from these systems fit the Higuchi model. Consequently, the release from these systems occurred through diffusion according to Fick's law.

Except the mentioned four samples, the release profiles were fitted with the Korsmeyer-Peppas model. The values of  $n$  (diffusion exponent) were between 0.08 and 0.422 (for all samples), which was less than 0.45 (critical value). Thus, dissolution from these systems was based on quasi-Fickian diffusion [70-71]. The complexity of systems that behave very similar to Fick's first diffusion law was presumably due to molecular interactions and microstructural heterogeneities [72-73].

### **3.3. Partial conclusions**

The prepared porous aggregate structures proved to be advantageous in terms of drug loading (with adsorption efficiency of 95-99%) and ensured effective drug binding. Drug release showed regular behavior in most cases. The *in vitro* experimental data were best fitted to the Higuchi and Korsmeyer-Peppas models. Fickian diffusion or quasi-Fickian Doxy diffusion from different  $\beta$ -TCP carriers (regardless of their chemical composition) could be controlled by the initial drug content of the system. The values of the Higuchi ( $k_H$ ) and Korsmeyer-Peppas ( $k_{KP}$ ) constants confirmed a significant decrease in the release rate by increasing the drug content of the sample.

On the other hand, a higher release rate could be achieved with a low drug loading. In this case, the retard effect of ion doping was also demonstrated. The presence of both Mg and Si in the carrier improved prolonged and sustained drug release.

Overall, the present research part highlighted that with simple methods such as ion substitution or changing the initial drug content of the system,  $\beta$ -TCP-based drug delivery systems can be easily adapted to meet different therapeutic needs.

## **4. The impact of hydroxyapatite-based biomaterials' chemical composition and morphology on their drug release characteristics**

### **4.1. Experimental part**

This present research part is a comparative study focusing on the release of antibiotics from different HA-based carriers. The release of Doxy was investigated based on the chemical composition of HA, its morphology, and the release media. Ion doping was carried out through a co-precipitation synthesis method. To create different morphologies, conventional oven drying and spray drying were used as drying techniques. The HA nanopowders and microspheres investigated primarily for drug delivery purposes were characterized using material characterization methods most commonly used in materials science (PSA, SEM, EDX, XRD, TG and DTA, BET). Drug release study was performed in SBF (simulated body fluid), and in PBS (phosphate-buffered saline) in a constant volume of 45 mL and at 37 °C and was measured spectrophotometrically.

### **4.2. Results and discussions**

#### **4.2.1. Particle size and morphological analysis**

During the particle size measurements, the following values were obtained for the HA, MgHA, HASi(1), and HASi(2) samples:  $686 \pm 417$  nm,  $681 \pm 464$  nm,  $574 \pm 390$  nm, and  $880 \pm 390$  nm, respectively. Regardless of the material's chemical composition, traditional drying resulted in particle agglomeration. The surface characteristics of HA produced by the co-precipitation method, coupled with insufficient electrostatic repulsion, led to particle adhesion [74-75]. As a result of agglomeration, parts with irregular morphology and size formed the bulk material.

By changing the drying technique to a mini spray dryer for suspension spraying, samples with a regular spherical morphology were obtained. It is evident from the images that the microspheres were not organized into agglomerates, they have well-defined edges. The surface of these microspheres has a very interesting morphology, characterized by a non-uniform, cauliflower-like structure (**Figure 23**). The achievement of the interesting morphology was facilitated, on the one hand by the operating parameters of the atomizer. On the other hand, the thorough preparation of the sample to be dried and the achievement of a sufficiently fine and homogeneous suspension contributed to the success of the production of uniform samples [74].

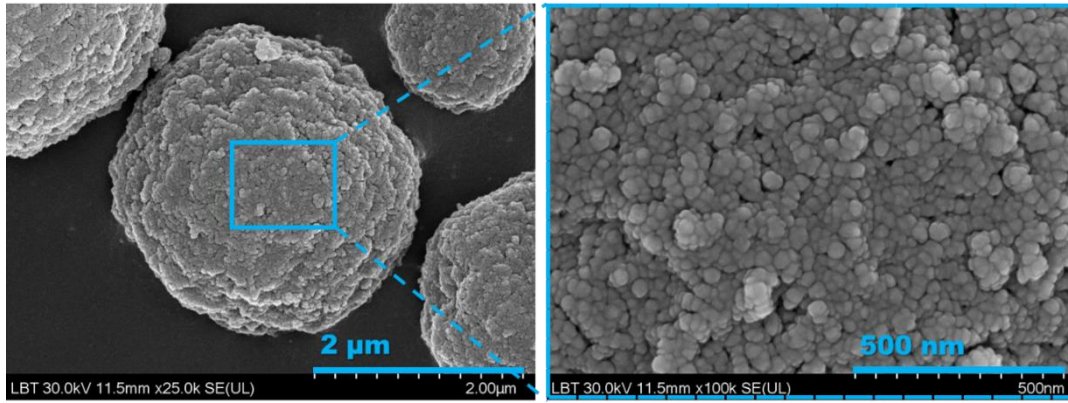


Figure 23: The cauliflower-like structure of HA\_M

#### 4.2.2. Determination of Doxy content

The drug loading of the produced and characterized samples was carried out by physical adsorption, with four starting Doxy solutions of different concentrations for each sample. The experiments were repeated three times, and the average values of the adsorption capacity were presented in the bar charts of Figure 26.

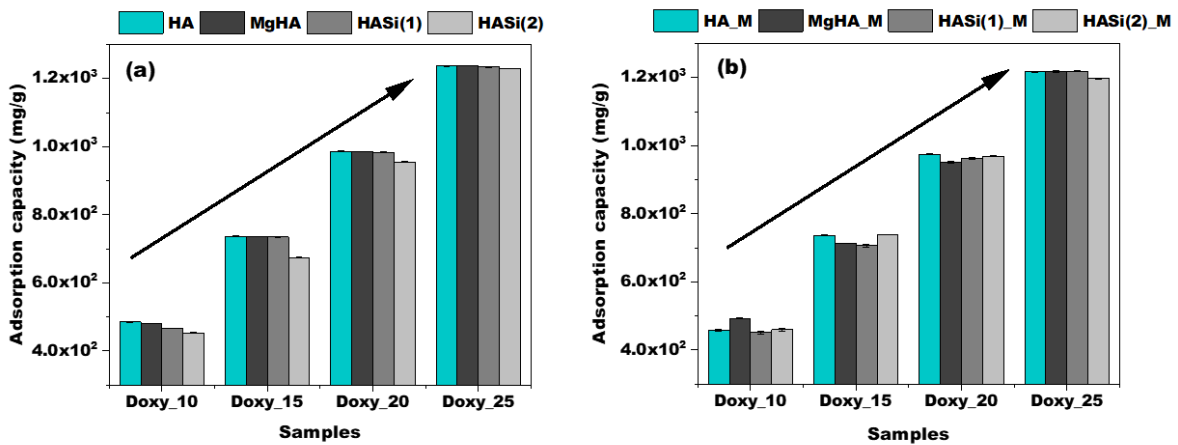
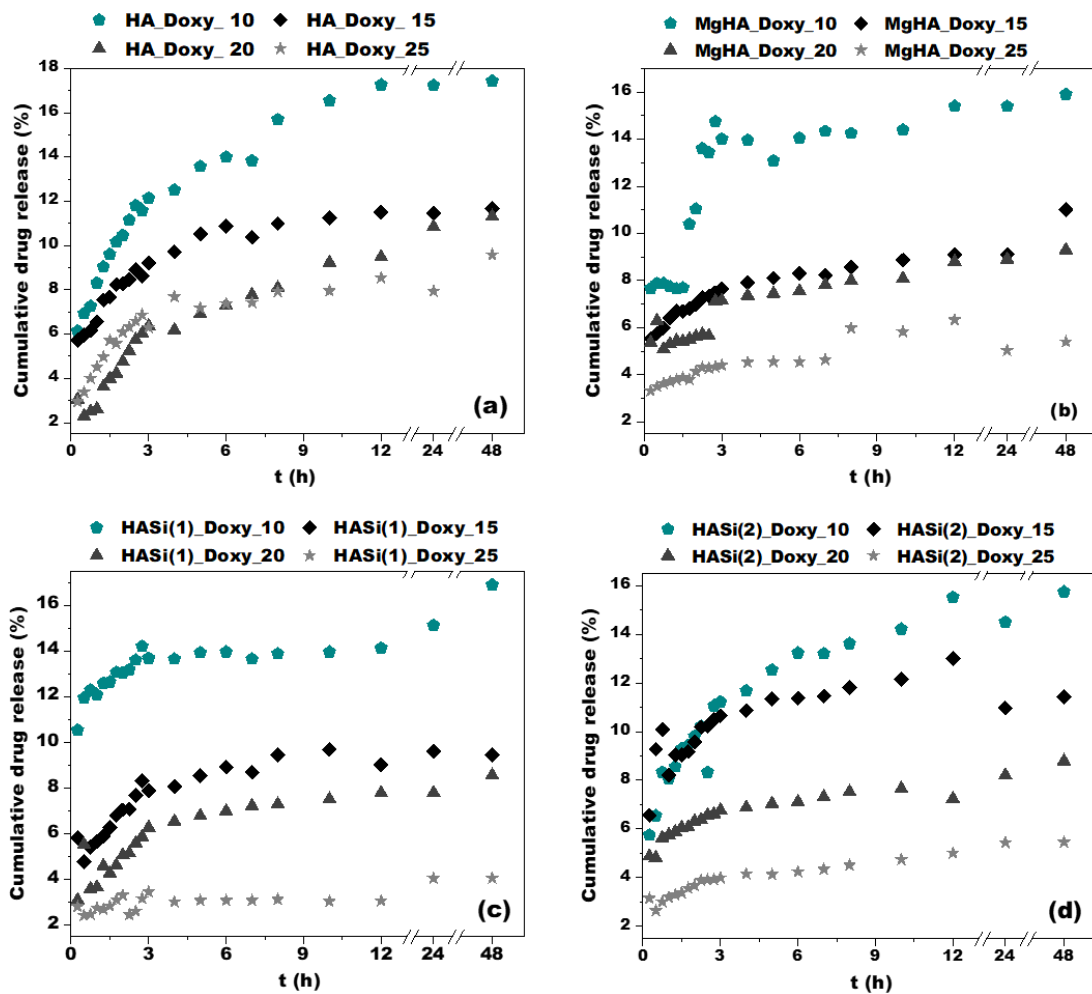


Figure 26: The adsorption capacities of the samples grouped according to their morphology ((a) irregular particles and (b) regular microspheres), and the concentration of the initial Doxy solution used for adsorption

Doxy showed a high affinity for CaP, and the adsorption capacity of the carrier was mainly dependent on the drug concentration ( $\geq 450 \text{ mg} \times \text{g}^{-1}$  for samples carrier\_Doxy\_10 and  $\geq 1200 \text{ mg} \times \text{g}^{-1}$  for samples carrier\_Doxy\_25). The increase in this value is well-correlated with the increase in the Doxy content of the samples [76].

The relatively low crystallinity of the carriers proved to be advantageous [77] in terms of adsorption capacity. Samples with similar crystallinity (HA, MgHA, and HASi(1)) showed similar drug loading, while the adsorption capacity of HASi(2) was lower. This could be explained by the high crystallinity of the carrier [78], which adversely affected the process.

### 4.2.3. Doxy release from HA-based nanopowders



**Figure 28:** Profiles of Doxy release from (a) HA, (b) MgHA, (c) HASi(1), and (d) HASi(2) carriers, based on initial drug content

The Doxy release profiles in SBF were similar to the dissolution profiles measured for  $\beta$ -TCP-based systems. However, significant differences in the amount of Doxy released were observed. The cumulative drug release percentage for HA-based samples was much higher and HA powders with different chemical compositions showed more favorable drug release.

The release profile could be divided into two well-distinguishable stages, which were characterized by different release rates based on the change in slope of the curves. Practically, from the initial moment of soaking, the first 4-hour period was determined by the rapid release of Doxy molecules less bound on the surface [79-80]. This phenomenon is common in the case of drug-loaded samples produced by adsorption [67, 81]. The second stage of release (from 4 to 48 hours after soaking) was characterized by a much slower release, which was evidenced by a notable change in the curve slope and the reduced amount of Doxy [32].

A drug release profiles analysis showed that increasing the initial Doxy content led to a decrease in the burst release, which could be explained by the interactions between the stronger Doxy-Doxy molecules [76]. Moreover, the drug release from the DDS could be controlled by its initial drug content.

Ion substitution imparts a retard effect to the carrier. The active substance molecule can form a stronger interaction with both  $Mg^{2+}$  ions [82-83] and  $SiO_4^{4-}$  ion groups [68-69]. In the case of both Si- and Mg-containing carriers, the amount of Doxy released was up to 4% less.

#### 4.2.4. Doxy release from HA-based microspheres

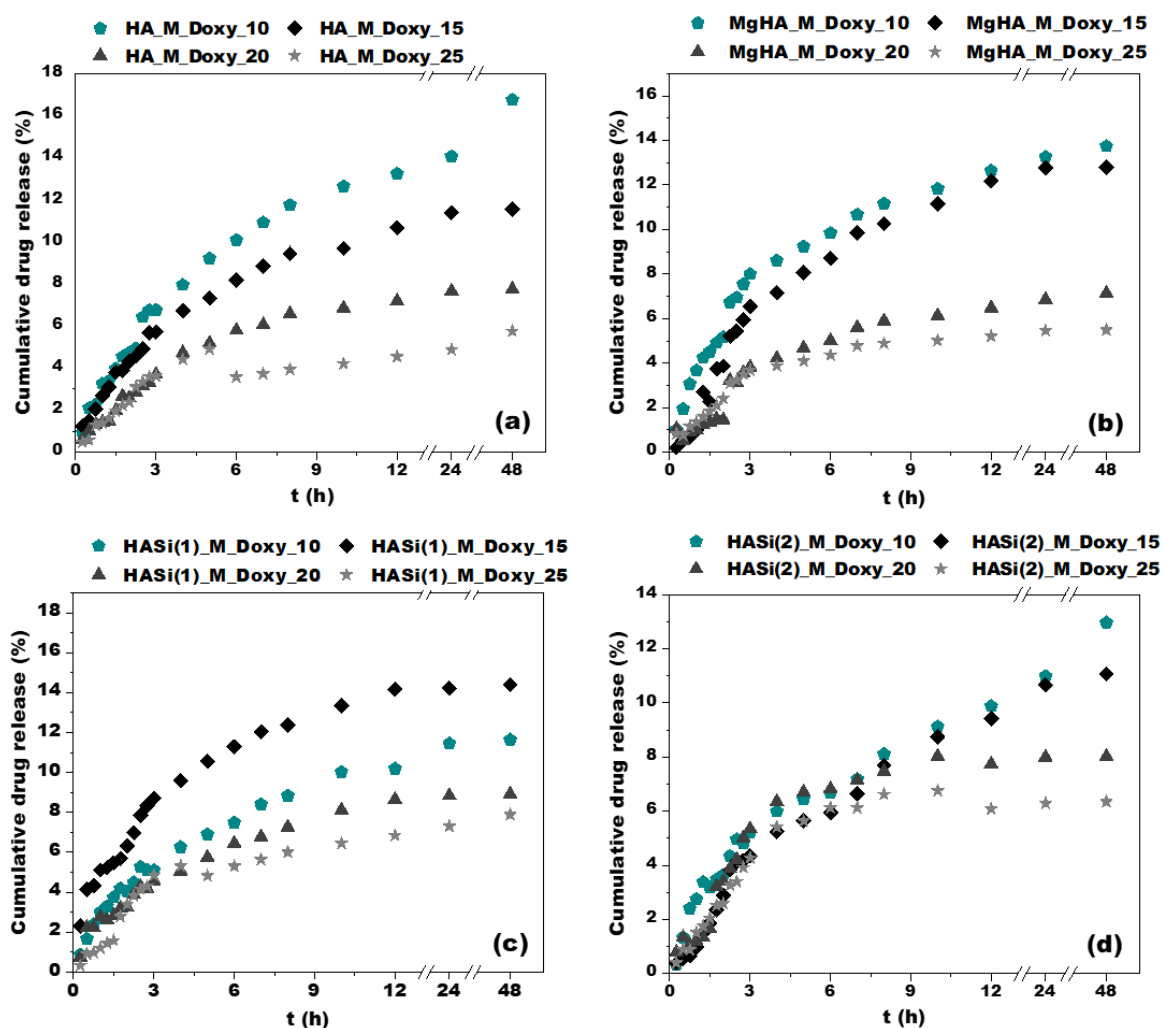


Figure 29: Release profiles obtained for (a) HA\_M, (b) MgHA\_M, (c) HASi(1)\_M, and (d) HASi(2)\_M microspheres with different Doxy contents

Similarly, in the case of carriers with microsphere morphology and different chemical compositions, the increasing tendency of the profiles over time and the dependence of the amount of Doxy released on the initial Doxy content could be highlighted.

The two release stages were well defined. The burst release stage was much more gradual and continuous than in the case of nanopores. There was no sudden initial jump; each dissolution profile started from 0 or close to 0. The profiles plotted as a function of the initial drug content did not deviate significantly from each other.

The systems studied and discussed in this section showed a more regular and pronounced retard effect than nanometric powder-based systems. Compared to agglomerates, the energetically more uniform spherical surface and the cauliflower-like porosity enabled the formation of stronger secondary interactions between Doxy and the given carrier [84]. The nature of these interactions determined the release and led to a slower release rate [78], which was true not only for the overall release profile but also for the burst stage.

The delayed release due to the presence of  $Mg^{2+}$  and  $SiO_4^{4-}$  groups was observed only in samples with low initial Doxy content. However, since this effect due to ion substitution was not clearly demonstrated at higher Doxy loadings (while it was visible in the case of completely asymmetric nanopore-agglomerates), the morphology proved to be crucial [76].

#### **4.2.5. Effect of release media on Doxy release**

The release of the active substance in PBS was much more intense and had a higher release rate than in SBF, as shown by the distinct upward trajectories of the release curves. An interesting observation was that the Doxy release from the nanopowders did not show a sudden increase from the 0th moment of soaking, the process was characterized by a gradual and continuous increase (in terms of the amount of released Doxy).

The release of Doxy in PBS was more regular, and the trends of the curves were different. These observations were further supported by subsequent kinetic calculations. The improved properties of the regular spherical morphology and drug delivery compared to the irregular powder agglomerates were highlighted.

During the soaking of bioactive materials in SBF, in addition to the drug release, another process typically occurs, characterized by ion exchange and crystal formation steps leading to the formation of a new apatite layer [85]. The system's pH variation was monitored. According to our assumption, the adsorption and ion exchange processes in SBF played a role in preventing the rapid release of Doxy molecules, so less Doxy could diffuse over time than in PBS [86].

#### 4.2.6. Discussion of Doxy release profiles from different carriers

The changes in drug transport were examined based on the chemical and morphological properties of biomaterials. **Table 10** presents the results of the regression analysis of the release data of the samples with the lower Doxy content.

Based on the highest  $R^2$  value, the key influence of morphology on the Doxy release was clearly confirmed. The release from powder agglomerates followed the Korsmeyer-Peppas model, while HA powders with modified morphology and composition showed Higuchi release.

As in the case of  $\beta$ -TCPs, the structural heterogeneity of the nanopowder carriers increased the complexity of various interactions (e.g. the orientation of the Doxy molecule on the surface). The values of  $0.067 < n < 0.28$  showed that the diffusion of drug molecules could not be perfectly described by Fick's first law [87]. The diffusion coefficients, regardless of the chemical composition of the carrier, were low and indicated the influence of an external physico-chemical phenomenon other than the release process [76,88]. In the case of these systems, quasi-Fickian diffusion took place.

The ion doping did not have a significant impact on the Doxy diffusion process, in the sense that the release mechanism did not change for the discussed samples. The ion incorporation played a role in the retard effect on the release. For carriers with regular spherical morphology and controlled release, the Higuchi constant values for Si and Mg-containing HA were lower than that of pure HA\_M, which also supports the retard effect. Based on these results, in SBF, Fickian drug diffusion could be easily achieved by morphological modification of the biomaterial [89-90].

**Table 10:** Kinetic modeling of drug release profiles obtained in SBF

Samples	Mathematical model						
	<i>Hixson-Crowell</i>		<i>Higuchi</i>		<i>Korsmeyer-Peppas</i>		
	$R^2$	$k_{HC}$	$R^2$	$k_H$	$R^2$	$k_{KP}$	$n$
<i>HA_Doxy_10</i>	0.899	0.014	0.969	3.743	<b>0.984</b>	8.588	0.280
<i>HASi(1)_Doxy_10</i>	0.5348	0.002	0.660	0.918	<b>0.838</b>	12.370	0.067
<i>HASi(2)_Doxy_10</i>	0.878	0.011	0.941	3.101	<b>0.950</b>	8.167	0.251
<i>MgHA_Doxy_10</i>	0.523	0.010	0.685	2.969	<b>0.745</b>	9.206	0.233
<i>HA_M_Doxy_10</i>	0.931	0.016	<b>0.987</b>	4.457	0.980	2.997	0.670
<i>HASi(1)_M_Doxy_10</i>	0.943	0.012	<b>0.991</b>	3.216	0.975	2.678	0.597
<i>HASi(2)_M_Doxy_10</i>	0.943	0.011	<b>0.982</b>	3.023	0.884	2.131	0.709
<i>MgHA_M_Doxy_10</i>	0.876	0.014	<b>0.962</b>	4.002	0.951	3.384	0.620

### **4.3. Partial conclusions**

The *in vitro* release studies have shown that the amount of cumulative drug release could be significantly influenced by changing the initial drug content of the system. High drug loading systems showed anomalous diffusive drug transport due to strong drug-drug interactions.

The degree of release was also influenced by the presence of foreign ions (e.g., significantly less Doxy was released from the Mg-containing carrier than from the pure HA carrier) and the ion concentration of the release medium. The presence of both Si and Mg resulted in a retard effect. The role of morphology proved to be crucial, carriers with an energetically more uniform surface (the microspheres) enabled a more regular Doxy release. The release of Doxy from these structures occurred gradually. Based on kinetic calculations, they showed Fickian diffusion in SBF. Due to the surface chemistry of the carriers, strong interactions were formed, suggesting a prolonged and sustained release. This was confirmed by the 15-day release studies conducted in PBS.

## **5. Investigation of optimized poly(lactic acid)/hydroxyapatite/ doxycycline coatings on titanium alloy surfaces**

### **5.1. Experimental steps**

The main goal of this research was the preparation and optimization of porous PLA and PLA/HA coatings, in order to achieve control and sustained Doxy release. The optimization of the coatings prepared with the dip coating technique focused on the parameters influencing the change in the average pore size and film thickness of the coatings. Box-Behnken response surface methodology (RSM) was used to optimize the operational parameters. Three-factorial and three-level design was selected, where the concentration of PLA solution (A), withdrawal rate (B), and immersion time (C) were the independent variables. In order to achieve the maximum average pore size and maximum film thickness, the value of each operating parameter was defined. The accuracy of the model was checked also experimentally on the obtained parameters. After that, the drug-containing composite coatings were prepared also using the optimal operating parameters. The coatings were characterized by SEM, EDX, TG and DTA. The thickness was measured with an Elcometer 456, and the wettability was also investigated. The corrosion behaviour was examined by potentiodynamic polarization (PP) and electrochemical impedance spectroscopy (EIS) measurements. The diffusion-controlled sustained drug release was demonstrated for 21 days.

### **5.2. Results and discussion**

#### **5.2.1. Optimization study**

According to the Box-Behnken design matrix (15 run), the morphology of the prepared coatings was examined using SEM. Open-pore coatings were formed in each run. The pore size distribution, as well as the average pore size, varied as a function of the examined independent variables. The choice of relatively high-concentration PLA solutions proved to be appropriate, as the viscosity of these solutions was sufficient to stabilize the condensed water vapour droplets responsible for pore formation on the surface [91].

The thickness of these coatings was also investigated. The lowest PLA concentration solution resulted in the preparation of the thinnest film (20.31  $\mu\text{m}$ ), while the thickest film was 46.58  $\mu\text{m}$ . The high viscosity of the polymer solution favored the preparation of thicker coatings [92-93].

Based on these experimental results and using the general second-order polynomial equation, the following regression response function was obtained for the average pore size:

$$d_{av.pore}(\mu m) = 2.2813 + 0.3628 * conc + 0.033 * v + 0.129 * \tau - 0.2378 * conc^2 + 0.1052 * v^2 + 0.0292 * \tau^2 + 0.0237 * conc * v - 0.0748 * conc * \tau - 0.1618 * v * \tau \quad (22)$$

Similarly, another response function could be generated for the change in coating thickness:

$$THK(\mu m) = 33.463 + 10.616 * conc + 0.658 * v - 1.326 * \tau - 1.988 * conc^2 + 0.290 * v^2 + 0.992 * \tau^2 + 2.265 * conc * v - 1.262 * conc * \tau - 2.685 * v * \tau \quad (23)$$

The equation obtained for pore diameter variation gave an R-squared value of 99.16%, while for film thickness, it was 99.11%. In other words, the model fits the experimental data well, with only about 0.9% of the variations could not be interpreted with the model. The importance of the models was also proven by the adjusted R-squared values ( $R^2_{adj} = 97.65\%$  for the pore size and  $R^2_{adj} = 97.52\%$  for the thickness, respectively). Naturally, the direction of the parameter's effect is defined by the sign of the coefficient [94].

The statistically significant effects of the independent variables were examined using ANOVA test. The Pareto diagram reproduced from these results were presented in **Figure 40**. Any factor whose column intersected the reference line at the value of 2.57 was considered a significant factor.

Taking into account the effects of the factors, the concentration of the dipping solution proved to be a crucial parameter in the formation of spontaneously microporous polymer coatings. A high concentration could, also, be resulted in the preparation of thicker coatings. For the thicker film, the drying time was longer, essentially indicating an increased solvent evaporation period while condensation was still occurring. This probably resulted in the coalescence of several multiple small droplets, leading to the formation of larger voids at the end of the drying process [95].

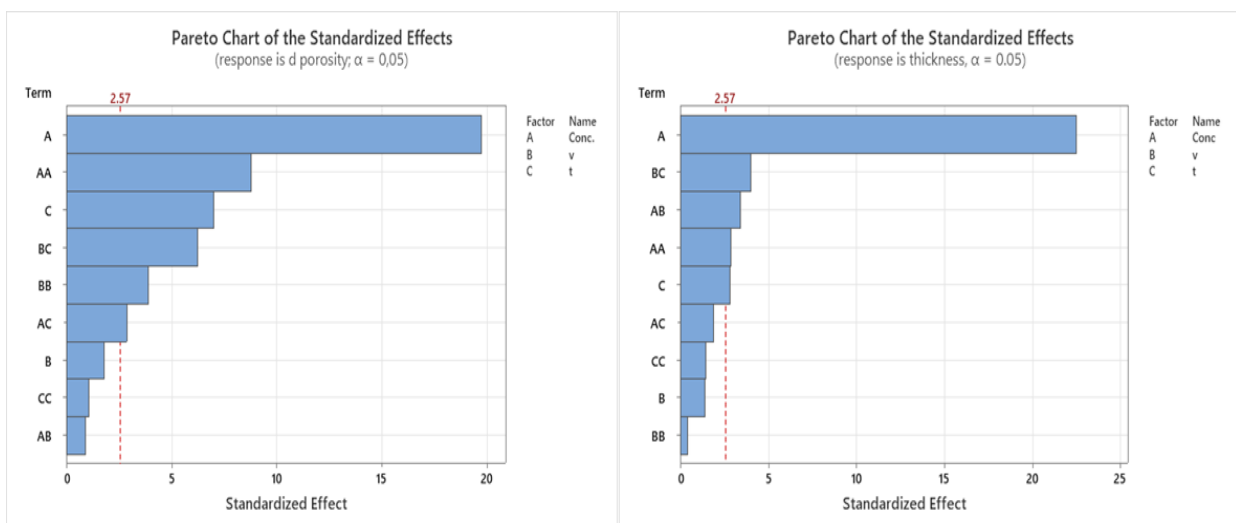


**Figure 40:** Pareto plot of the standardized factors ( $\alpha = 0.05$ )

After a detailed discussion of the accuracy and suitability of the models, the levels of the independent variables that result in the achievement of the maximum average pore size and maximum thickness in the range of experimental limits were determined. The thickness of the coating played a crucial role in drug loading. Studies have demonstrated that thicker coatings were suitable for preparing formulations with higher drug content [96]. According to the summarized results in **Table 18**, increasing the concentration of the PLA solution, maintaining a high withdrawal rate, and minimizing immersion time lead to the maximization of the investigated parameters. In the following, both HA and Doxy-containing coatings were prepared under these experimental conditions.

**Table 18:** Optimal levels for max.  $d_{av. pore}$  and max. thickness

<i>conc.</i> (wt %)	<i>v</i> (mm/min)	<i>τ</i> (s)	<i>calculated <math>d_{av. pore}</math> (<math>\mu\text{m}</math>)</i>
11.87	150	0	2.7
12	150	0	<i>calculated thickness</i> ( $\mu\text{m}$ ) 51.57

### 5.2.2. Morphological characterization of coatings

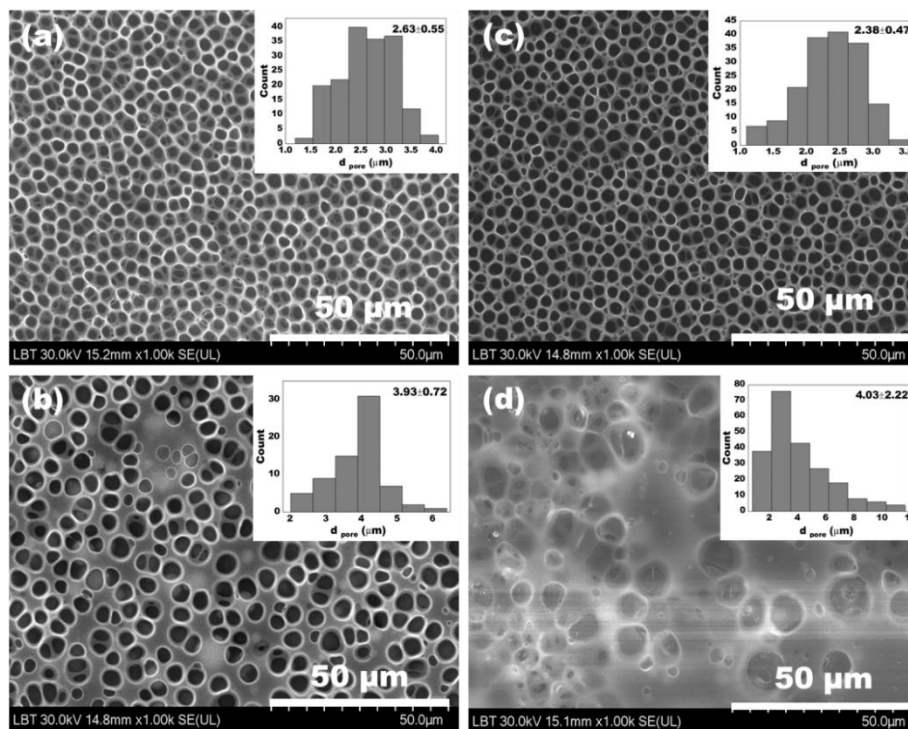


**Figure 44:** SEM images and the corresponding pore size distribution of (a) PLA, (b) PLA\_HA, (c) PLA\_D5, and (d) PLA\_HA\_D5

The coatings with different compositions have different porosity. As expected after the optimization study, the pure PLA coating had ordered porosity and was crack-free. The pore

size fell within a narrow range, and a relatively regular pore size distribution was observed. The average pore size was  $2.63 \pm 0.55 \mu\text{m}$ . This value was very close to the calculated average pore diameter of  $2.7 \mu\text{m}$ , which indicated the reproducibility of the results obtained during the experimental design.

The addition of HA microsphere to the PLA dipping solution led to an increase in the average pore size. The quantity of 10 wt% resulted in a noticeable increase in the viscosity of the polymer solution, which delayed the solvent evaporation time, thereby facilitating the formation of larger pores.

### 5.2.3. In vitro corrosion behaviour

The lifetime of implants, calculated from the time of their insertion into the body, is greatly influenced by their corrosion resistance [97]. In this study, the corrosion properties of PLA and PLA\_HA-based coatings were examined using PP and EIS. The main corrosion parameters obtained by extrapolation of Tafel curves are presented in **Table 19**.

**Table 19:** Significant corrosion parameters derived using the Tafel extrapolation method based on the PP curves

Sample	$E_{\text{OCP}}$ (V)	$\frac{E_{\text{corr, obs/}}}{E_{\text{corr, calc}}}$ (V)	$I_{\text{corr}}$ (A)	$i_{\text{corr}}$ (A/cm <sup>2</sup> )	$\beta_{\text{c}}$ (V/dec)	$\beta_{\text{a}}$ (V/dec)	$R_{\text{p}}$ ( $\Omega$ )	corr. rate (mm/year)
PLA_HA	-0.064	-0.097	$7.708 \times 10^{-8}$	$3.083 \times 10^{-7}$	0.043	0.045	10930	$7.40 \times 10^{-3}$
PLA_HA_D2.5	-0.097	-0.098	$3.280 \times 10^{-8}$	$1.312 \times 10^{-7}$	0.02	0.021	5520	$3.15 \times 10^{-3}$
PLA_HA_D5	-0.088	-0.213	$6.498 \times 10^{-8}$	$2.599 \times 10^{-7}$	0.062	0.044	18300	$6.24 \times 10^{-3}$
PLA_HA_D7.5	-0.174	-0.194	$2.298 \times 10^{-8}$	$9.192 \times 10^{-8}$	0.01	0.009	1757	$2.21 \times 10^{-3}$
PLA	0.017	0.01	$1.071 \times 10^{-8}$	$4.283 \times 10^{-8}$	0.046	0.041	76900	$1.03 \times 10^{-3}$
PLA_D2.5	-0.095	-0.102	$3.344 \times 10^{-9}$	$1.338 \times 10^{-8}$	0.036	0.034	158800	$3.21 \times 10^{-4}$
PLA_D5	-0.006	-0.043	$4.656 \times 10^{-9}$	$1.862 \times 10^{-8}$	0.07	0.074	478600	$4.47 \times 10^{-4}$
PLA_D7.5	-0.033	-0.058	$1.427 \times 10^{-9}$	$5.707 \times 10^{-9}$	0.044	0.053	718700	$1.37 \times 10^{-4}$

In general,  $i_{\text{corr}}$  is the most significant parameter in the characterization of the corrosion process. As is well known, a high  $i_{\text{corr}}$  value indicates a rapid corrosion rate [98]. According to the values in **Table 19**, the pure PLA layer provided better corrosion resistance compared to the PLA\_HA coating.

Our experiments showed that the addition of HA to the PLA solution led to the formation of coatings with an increased average pore size (see **Figure 44**). Larger pores created sites

where SBF could accumulate. Consequently, this allowed for enhanced permeation of various ions, such as  $\text{HCO}_3^-$ ,  $\text{Cl}^-$ , and  $\text{HPO}_4^{2-}$  ions [99]. Due to the conducting species from the electrolyte, the coating exhibited lower resistance [100]. In addition, the lower corrosion resistance was attributed to the surface hydrophobicity [101].

Similarly, it was observed that coatings containing Doxy showed better corrosion protection properties than those without Doxy. This suggested that Doxy had an inhibitory effect on corrosion. Based on our observations, it was noted that as the Doxy content in the coating increased, the layer more effectively hindered the electrolyte from reaching the metal surface [102]. The corrosion rate reduction caused by the drug was facilitated by the thickness of the coatings [103], which increased with increasing Doxy content

#### 5.2.4. Investigation of Doxy release

The average release profiles were presented in **Figure 51**. Most of the release profiles exhibited similar behavior throughout the entire observation period. Unacceptable, irregular behavior was not observed in any case. The behavior of the coatings during soaking in SBF was characterized by a continuous release of Doxy in all instances. In the first 12 hours of the experiment, a burst drug release characteristic of polymer systems [104-105] was observed, followed by a sustained release phase. In most samples, after the first day, the drug release rate decelerated, and the amount of released drug increased only slightly. Based on these observations, the ordered porous coatings provided consistent and controlled Doxy release. Moreover, the reproducibility of the *in vitro* behavior of the coatings was high, with low variances among individual measurements.

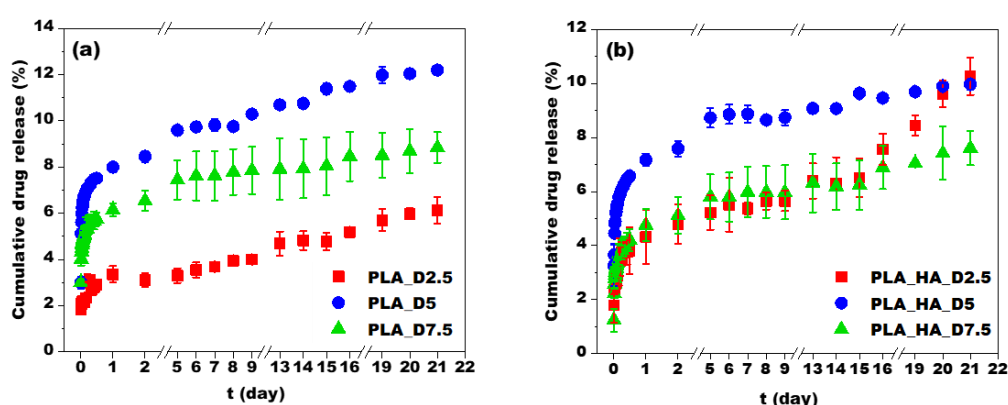


**Figure 51:** Doxy release from (a) PLA and PLA\_HA coatings

The high affinity between HA and Doxy was also observed in this study. The HA-containing coatings showed retard behavior compared to pure PLA-based coatings. Due to the secondary bonds and electrostatic attraction, the amount of released drug was reduced [106].

Doxy has the ability to form a chelate complex with the  $\text{Ca}^{2+}$  ion present in HA, so the affinity between the two compounds is high [107]. However, the hydrophobic nature of the polymer layer also contributes to the achievement of sustained release [108].

### 5.2.5. Release kinetics study

In the case of biodegradable systems, drug release is often a complex and intricate process. Almost all investigated coatings resulted in the highest  $R^2$  with the Korsmeyer-Peppas model. Its graphic representation is presented in **Figure 52**. The PLA\_D2.5 coating stands as an exception, where the first-order kinetic model yielded the highest  $R^2$  value.

During the investigation period, the coatings did not undergo significant damage that could have affected the Doxy release [109]. The release was controlled by the Fickian diffusion of Doxy molecules from the coating. Compared to the driving force of diffusion, the degree of relaxation of the polymer chain was minimal during the examined period [110]. The relatively small quantity of released drug supports the assumption that polymer degradation was not significant over 21 days.

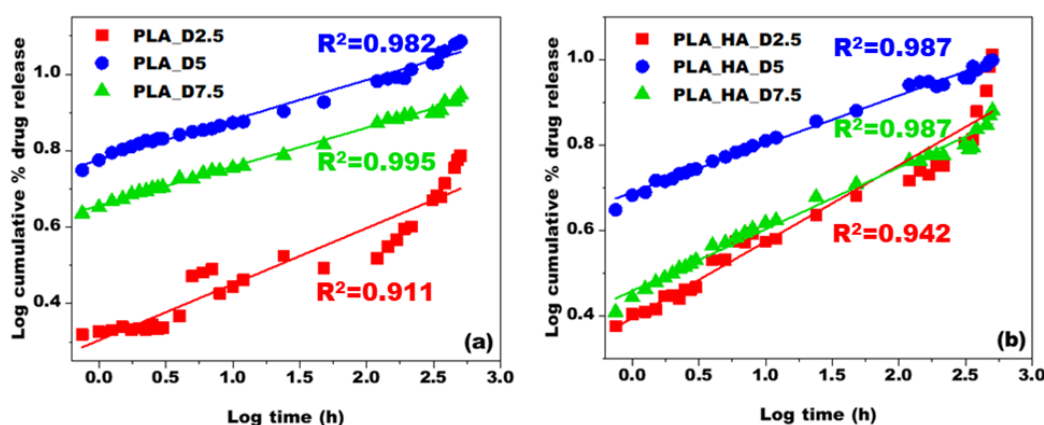


**Figure 52:** Release data fitted to the Korsmeyer-Peppas model to describe the release kinetics of Doxy from (a) PLA and (b) PLA-HA coatings

### 5.3. Partial conclusions

The combination of metal implants with DDSs has proven to be promising from a therapeutic perspective. Well-organized, open-porous PLA, and PLA\_HA coatings with homogeneous HA distribution were prepared using the dip-coating method on a Ti6Al4V substrate. The porosity and thickness of the coatings are crucial parameters in terms of drug release, corrosion resistance, and bioactivity. The changes in the concentration of the PLA solution resulted in the most significant differences in the targeted parameters. Keeping the concentration and withdrawal rate at their maximum value resulted in coatings with maximum average pore diameter and thickness within the investigated experimental parameters.

The electrochemical investigations indicated that porosity plays a crucial role in corrosion resistance, as large pores favored corrosion processes. Moreover, Doxy proved to be a potent inhibitor, both for PLA and PLA\_HA coatings.

*In vitro* drug release studies in SBF confirmed the sustained Doxy release controlled by diffusion from the coatings. The relatively long duration (21 days) of the unchanged release mechanism indicated the stability of the coatings.

## 6. Real-time investigation of Doxycycline release by electrochemical method

### 6.1. Experimental steps

The objective of this research part was to innovate *in vitro* measurements by **real-time monitoring** of the release profile and comparing the results with values obtained through spectrophotometric methods. Among the electrochemical methods, the differential-pulse voltammetry (DPV) method was used to eliminate sampling. The method's applicability was investigated for carriers with new morphologies, such as Doxy-loaded PLA and PLA/HA nanofibers. Both PLA and PLA/HA nanofibers were produced using the electrospinning method. The drug loading of PLA and PLA/HA nanofibers was carried out during physical adsorption using aqueous Doxy solutions with initial concentrations of 3, 7, and 12  $\text{g}\times\text{L}^{-1}$ . The nanofibrous carriers were characterised using SEM, EDX, and FTIR techniques. Both cyclic voltammetry (CV) and differential pulse voltammetry (DPV) measurements were conducted in an undivided three-electrode cell setup. Following the traditional cell configuration, an Ag/AgCl,  $\text{KCl}_{\text{sat}}$  reference electrode, a platinum wire auxiliary electrode, and a glassy carbon (GCE) working electrode were used.

### 6.2. Results and discussion

#### 6.2.1. Investigation of the electrochemical behaviour of Doxy

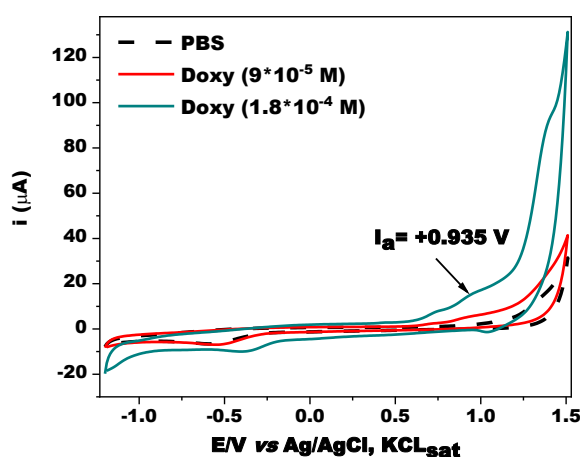


**Figure 57:** CV measurements at the GCE with and without Doxy. Experimental setting: electrolyte, 0.1 M PBS (pH = 7); starting potential, -1.2 V vs. Ag/AgCl,  $\text{KCl}_{\text{sat}}$ , scan rate, 50 mV/s.

In order to be able to monitor the drug release *in situ*, using an electrochemical method, the electrochemical behavior of the active substance must be known. For this, in the first step, CV was performed to study the redox behavior of Doxy, followed by optimization of the operating parameters of the DPV. Finding and applying optimal parameters are crucial for carrying out sufficiently sensitive and reliable measurements.

The tricarbonyl, dimethylammonium, and phenolic-diacetone groups of the Doxy molecule are ionizable groups. Due to this, typically three oxidation peaks appear in the voltammograms (depending on the pH) [111]. As shown in the cyclic voltammograms presented in **Figure 57**, at pH around neutral these peaks merge [111]. Regardless of the concentration of the Doxy solution, the anodic peak ( $I_a$ ) attributed to the oxidation of the molecule was identified at a potential of +0.935 V vs. Ag/AgCl,  $KCl_{sat}$ .

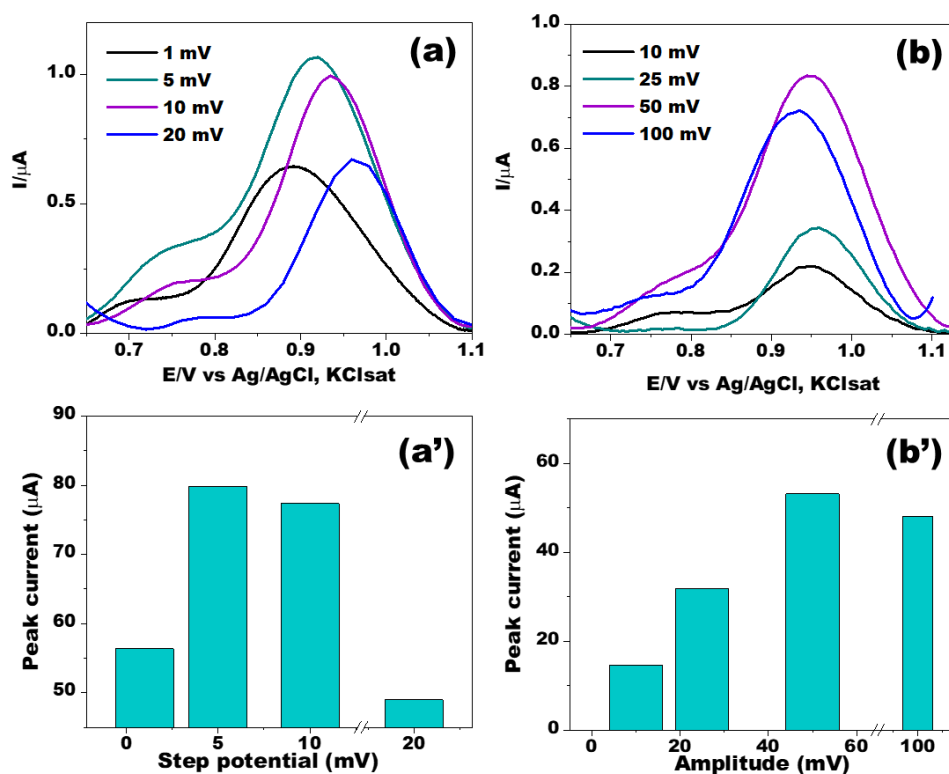


**Figure 58:** Changes of the DP voltammograms recorded on the GC electrode and the corresponding anodic peak currents in the presence of Doxy ( $1.4 \times 10^{-4}$  M), with variations in the step potential (a, a') and the pulse amplitude (b, b'). Experimental setting: 0.1 M PBS (pH= 7) as the electrolyte; 50 mV pulse amplitude; 5 mV step potential; +0.7 V vs. Ag/AgCl,  $KCl_{sat}$  as the starting potential.

The sensitivity of the DPV method depends on the input parameters, so an optimization study was carried out for the step potential and pulse amplitude. Based on these results (see **Figure 58**), a step potential of 5 mV and a pulse amplitude of 50 mV were found to achieve the maximum peak current for the desired sensitivity and measurement stability [112]. Consequently, these parameters were used for further investigations.

### 6.2.2. Real-time release study of Doxy

From the nanofibrous systems, regardless of their chemical composition, similar Doxy release was observed as those discussed so far. Although we are dealing with different carriers

both in terms of morphological and material quality, two phases of the release profile can be distinguished: an initial burst release followed by a sustained section (see **Figure 62**). The burst release was favored by several parameters. Firstly, as discussed earlier, weak secondary interactions quickly broke down, resulting in a relatively high initial release due to rapid diffusion [113]. Secondly, the properties of the Doxy molecule, such as its high affinity for aqueous media and the recrystallized form after adsorption, also influenced the initial stage of release [113-114].

For both carriers, predominantly, fibers larger than 500 nm composed the electrospun mats. Larger fiber diameters have been demonstrated to play a role in constant and prolonged release [115]. Comparing the drug-delivery properties of HA-containing PLA fibers with those of pure PLA fibers, it was observed that in some cases, 2-5 % less diffused Doxy was measured from the pure PLA carriers. Since the encapsulation of HA in the nanofibers did not cause any apparent morphological changes, the fiber diameters may have been crucial.

### 6.2.3. Validation of the DPV method

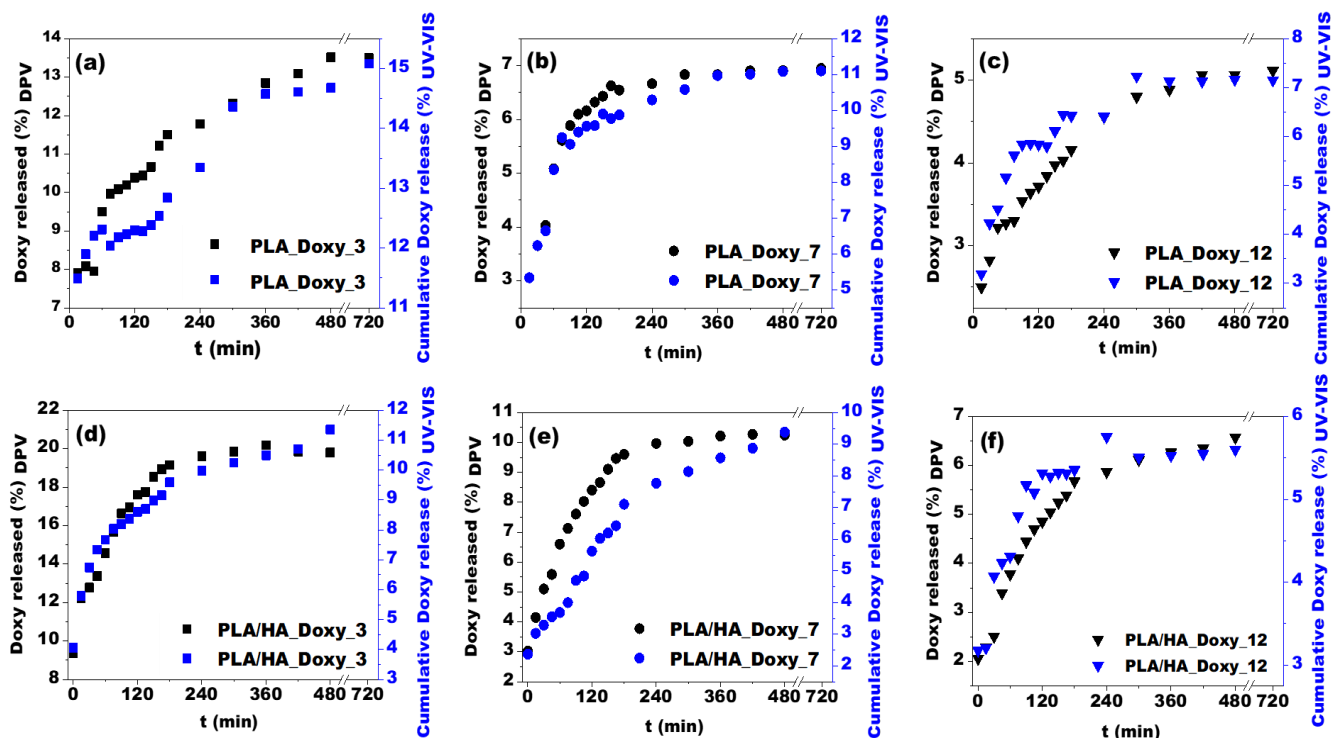


**Figure 62:** Doxy release profile measured by DPV (black scatter) and UV-VIS spectrophotometry (blue scatter) for (a) PLA\_Doxy\_3, (b) PLA\_Doxy\_7, (c) PLA\_Doxy\_12, (d) PLA/HA\_Doxy\_3, (e) PLA/HA\_Doxy\_7, and for (f) PLA/HA\_Doxy\_12 samples.

The results of the spectrophotometric measurement showed similar behavior and nearly identical Doxy diffusion tendencies as the data recorded with DPV (**Figure 62**). Of these, the

irregular drug release from the PLA\_Doxy\_3 and PLA/HA\_Doxy\_3 samples and the dependence of the release on the initial Doxy content should be highlighted.

For pure PLA nanofibers, it was observed that, according to DPV measurements, the released Doxy was about 1.6%, 4%, and 2% less than that determined by spectrophotometric measurements after the first 12 h of soaking. These differences were close to each other, suggesting that dilution associated with sampling during UV-VIS measurements influenced the release. Continuous replenishment with fresh PBS probably led to a change in concentration gradients and an increase in release rate. This observation was supported by the shift in the equilibrium state compared to the voltammetric release profiles [112]. One of the main reasons for the differences between the measured data series was the different sensitivity of the two methods [116]. Nevertheless, the application of DPV in this field proved to be successful, as it allowed the *in situ* measurement of Doxy diffusion from PLA-based electrospun mats without constant sampling and dilution. The method did not affect the monitoring of drug release and diffusion processes, so no shift in the equilibrium state was observed in the case of the profiles obtained with DPV. The voltammetric method was also advantageous due to its rapid measurement time.

### 6.2.3.1. Model-independent methodology

**Table 23:** Comparison of the release profiles obtained with the DPV and UV-VIS methods based on the difference- ( $f_d$ ) and similarity ( $f_s$ ) factors

Samples	$f_s$	$f_d$
PLA_Doxy_3	80	16.45
PLA/HA_Doxy_3	53.65	96.56
PLA_Doxy_7	72.2	36.56
PLA/HA_Doxy_7	79.71	38.27
PLA_Doxy_12	82.24	33.34
PLA/HA_Doxy_12	<b>95.35</b>	<b>4.42</b>

Following the graphical comparison, the Doxy release data of the investigated systems obtained by both methods were compared using a numerical method. The values of the determined similarity factors ( $f_s$ ) and difference factors ( $f_d$ ) were given in **Table 23** [112]. These parameters well reflected the observations discussed during the graphical comparison, where the profiles showed similar trends, but the measured amount of released Doxy was different. The data obtained for both PLA and PLA/HA electrospun mats, regardless of their initial Doxy content, met the criteria for  $f_s$ , as the values were greater than 50. The  $f_d$  values illustrated the differences in the percentage of cumulative Doxy release. This model-independent approach

demonstrated that the voltammetric method was suitable for real-time, *in situ* monitoring of Doxy diffusion [112].

### 6.2.3.2. Model-dependent methodology

Linear regression analysis performed with five models was fitted with both the UV-VIS and DPV release data series for the first 6 h of the study. The appropriate model was determined by the coefficient of determination.

Comparing the results, two observations could be emphasized. Firstly, the DPV technique has proven to be a successful alternative method for studying Doxy release. Secondly, the release of Doxy from all investigated nanofibrous systems followed the kinetics of the Korsmeyer-Peppas model [117]. The investigated systems were not fully Fick-type. Due to the nature of the active substance and the polymer, the diffusion from the nanofibrous systems differed from the linear one [22,112].

**Table 25:** The statistical analysis (ANOVA) of the release data of Doxy examined using the voltammetric and spectrophotometric methods and fitted with five different mathematical models.

Origin of variation	SS	df	MS	F <sub>crit</sub>	F	p-value
<b><i>R<sup>2</sup>-based single-factor ANOVA</i></b>						
0o, Io, HC, and H kinetic models	0.096783	7	0.013826	2.2490	1.2486	0.3001
0o, Io, HC, H, and KP kinetic models	0.223502	9	0.024834	2.0733	2.5004	0.0190
<b><i>k-based single-factor ANOVA</i></b>						
0o, Io, HC, H, and KP kinetic models	80.38197	9	8.93133	2.0733	<b>7.1450</b>	1.42×10 <sup>-6</sup>
<b><i>Two-factor ANOVA, with replication in terms of R<sup>2</sup></i></b>						
0o, Io, HC, H, and KP kinetic models	0.20871512	4	0.052179	2.5571	5.2538	0.0013
Investigation technique (DPV/ UV-VIS)	0.00903563	1	0.009036	4.0343	0.9097	0.3447
Interactions between investigation technique and kinetic models	0.0057515	4	0.001438	2.5571	0.1447	0.9644
<b><i>Two-factor ANOVA, with replication in terms of k</i></b>						
0o, Io, HC, H, and KP kinetic models	78.6933	4	19.67332	2.5571	15.7386	2.12×10 <sup>-8</sup>
Investigation technique (DPV/ UV-VIS)	0.257921	1	0.257921	4.0343	0.2063	0.6516
Interactions between investigation technique and kinetic models	1.430755	4	0.357689	2.5571	0.2861	0.8856

The stability of the carriers was indicated by the low amount of cumulative released Doxy, suggesting that in the first few hours, the polymer nanofibers did not undergo any

structural changes that would have significantly affected drug release. This also supported the diffusion-controlled mechanism.

Furthermore, a one-factor and two-factor replication ANOVA test was conducted to compare the models describing drug release. The tests were applied to both the release rate constants ( $k_0$ ,  $k_1$ ,  $k_{HC}$ ,  $k_H$ , and  $k_{KP}$ ) and the values of  $R^2$ .

The results of one-way analysis indicated that while fitting with the  $0_0$ ,  $I_0$ ,  $HC$ , and  $H$  models did not show significant differences ( $F = 1.25 < F_{crit} = 2.25$ ,  $p (=0.3) > 0.05$ ), the addition of  $KP$  to the ANOVA test resulted in significant differences ( $F = 2.5 > F_{crit} = 2.07$ ,  $p (=0.019) < 0.05$ ). The results of the same test for  $k$ -values showed significant differences. These findings were not surprising and resulted from the mathematical differences between the equations of the five different models.

The results of the two-factor replication ANOVA test for  $k$ -values and  $R^2$ -values were very similar, leading to similar conclusions regarding the analyzed data. The significant differences between kinetic models highlighted the mechanism of Doxy release. The differences between the two measurement methods were not significant, either in terms of  $R^2$  and  $k$  values ( $F < F_{crit}$ ,  $p > 0.05$ ). This observation supported the conclusions drawn from  $f_s$  and  $f_d$  values. The absence of interaction between the applied kinetic models and the measurement method was also confirmed by the  $F$  and  $p$  values.

### 6.3. Partial conclusions

It was possible to produce a drug delivery with a fibrous morphology imitating the extracellular matrix by electrospinning, which showed favorable properties in terms of drug release.

These experimental results contributed to the development of continuous, *in situ*, real-time monitoring of drug release. DPV proved to be a suitable alternative analytical method with numerous advantages. The method did not influence the release process, and the lack of sampling played a role in determining the real-time quasi-equilibrium state. This rapid, simple, and efficient method can be suitable for studying the release of electroactive group-containing drugs and improving the efficiency of LDDSs development.

### III. General conclusions

The topic of the research presented in this doctoral thesis was the investigation of biomaterials with different chemical compositions and morphologies as local drug delivery systems. Similar to other medical fields, in orthopedics and dentistry, LDDSs represent a new opportunity in treatments, infection prevention, and healing. My research is based on the design and development of systems that, in addition to being biocompatible and assisting the physiological healing processes, are suitable for the delivery of the drug at the therapeutic site. Through the targeted treatment, the efficacy of the active substance can be significantly increased, which results in a reduction in recovery time. The main aspect of the development of systems with different characteristics was to ensure controlled drug release and prolonged, even multi-stage release. The site, period, and drug release rate influence biological processes, so the design of LDDSs is based on these parameters.

Doxycycline (Doxy), which can be used to prevent various inflammations and infections, was tested in the case of four different types of carriers. The key question was to understand the release behavior of Doxy, determine the factors influencing the process, and define the drug release kinetics. In the case of LDDSs, the properties of the carrier as well as the interactions between the carrier and the active substance significantly influence the release rate of Doxy. Among the LDDS, the release profiles of Doxy were investigated for  $\beta$ -tricalcium phosphate ( $\beta$ -TCP) and silicon-, as well as magnesium-modified  $\beta$ -TCP (*Original contribution, Chapter 4*); for rounded nanopowder and microsphere morphology of hydroxyapatite (HA), Si- and Mg-doped HA (*Original contribution, Chapter 5*); for polylactic acid (PLA) and PLA coatings containing HA (*Original contribution, Chapter 6*); and for PLA and PLA/HA nanofibers (*Original contribution, Chapter 7*).

In the *first chapter* of the personal contribution, we aimed to investigate pure  $\beta$ -TCP and with silicon- or magnesium- substituted  $\beta$ -TCP as carriers for Doxy. The objectives of the research summarized in the chapter included the preparation and characterization of the aforementioned carriers, and the investigation of their properties as drug carriers *in vitro*.

1) The co-precipitation method followed by subsequent heat treatment proved to be suitable for achieving the pure  $\beta$ -TCP phase. The pH of the reaction mixture, the reaction time, the sintering temperature, and its duration were identified as key parameters affecting the material quality. The optimized experiments showed that the starting materials  $\text{Ca}(\text{NO}_3)_2$  and  $(\text{NH}_4)_2\text{HPO}_4$ , with a mixing time of 2 h at room temperature (pH= 8), followed by stepwise sintering up to 900°C, resulted in the formation of pure  $\beta$ -TCP phase.

2) The thermal transformation of calcium-deficient apatite is a multi-step process, the final step of which is greatly determined by the initial Ca/P ratio. The transformation temperature depends on the elemental composition of the sample.

3) The incorporation of foreign ions into  $\beta$ -TCP resulted in various crystallographic changes. Silicon doping led to less significant changes, while cationic substitution led to significant structural alterations.

a) The partial incorporation of Si, resulting in a change in the intensity of the X-ray diffraction patterns, was independent of the silicon source used during the reaction ( $\text{Na}_2\text{SiO}_3$  or Ludox AS-40).

b) The incorporation of  $\text{Mg}^{2+}$  was confirmed by the significant shift of the diffraction peaks (compared to pure  $\beta$ -TCP) and a decrease in crystallinity.

4) The powders arranged into porous aggregates had a significant adsorption efficiency, which enables outstanding drug loading. The process depended on the initial drug solution concentration.

5) Powders with porous aggregates, serving as carriers for Doxy, provide slow drug release *in vitro*. The drug release from  $\beta$ -TCP powders followed either Fickian diffusion (Higuchi model) or quasi-Fickian diffusion (Korsmeyer-Peppas model) mechanisms.

6) The diffusion of Doxy can be greatly controlled by the amount of initial drug content of the sample. Strong Doxy-Doxy interactions result in a decrease in release rate, which reduces the amount of drug released over time.

7) In addition to the drug loading level, the release rate can also be controlled through ion substitution. Compared to pure  $\beta$ -TCP, Mg-substituted  $\beta$ -TCP has a more retard effect, while the presence of Si in the structure of the carrier is even more significant. In this case, not only the release was more regular, but the cumulative drug release percentage was even 3-5% less at a given time.

These observations regarding the release of Doxy, the influencing parameters, and their impact were also examined in the case of HA and ion-substituted HA carriers (**Chapter 5**). Due to its biological properties, the use of HA is more widespread, however, the approach as a local drug carrier represents a novel area of research. The structural changes were also induced by the substitution with Si or Mg, using the same foreign-ion sources as in the fourth chapter's starting materials. The purpose of the experiment was to examine and discuss the differences between HA powders with different chemical compositions and morphologies, primarily from the perspective of drug carrier suitability.

8) The powders produced by co-precipitation were characterized by various material testing methods in accordance with material science requirements. The purity of the materials and the successful incorporation of foreign ions were supported by X-ray diffraction measurements.

a) In terms of crystal size, silicon facilitated crystal growth, the crystal size of Si-doped HA nanopowders was several tens of nanometers larger than that of pure HA.

b) The high concentration of  $Mg^{2+}$  used in the synthesis inhibited crystallization and crystal growth. In addition, a structural destabilizing effect was noticed, which turned out to be stronger compared to those observed in the previous experimental chapter. Compared to the pure HA carrier, MgHA showed 3% less crystallinity, while in the case of  $\beta$ -TCPs, it was little more than 1%.

9) The morphology of HA-based powders could be influenced by the drying method, as supported by the SEM images. Drying with a mini spray dryer resulted in the production of microspheres with regular spherical morphology. The cauliflower-like surface morphology of these spheres was not affected by material quality. The size distribution of the microspheres and the average particle diameter were similar for all samples.

10) The thermal behavior of the powders was independent of morphology and elemental composition, there were no significant changes in either the TG or DTA curve. The destabilizing effect of the incorporation of  $Mg^{2+}$  was also visible here, in the largest mass loss (18 % in the case of MgHA\_M, while 10 % in the case of HA\_M).

11) The presence of foreign ions significantly altered the porosity of the powder, the decrease in the pore diameter and the increase in the specific surface area were significant for both Si- and Mg-containing samples.

12) Porosity is a crucial issue not only in terms of physiological processes but also in terms of drug loading. The drug molecules not only bound on the surface, but also penetrated into the pores of the carrier.

13) The fourth and fifth chapters of the thesis emphasized the high affinity of the Doxy molecule to both CaP groups. A positive correlation was observed between high drug loading and initial drug solution concentration, in which the high affinity played a crucial role. Comparing the drug-loading properties of pure  $\beta$ -TCP and HA, it was found that HA had a higher adsorption capacity. This observation was especially significant in the case of lower Doxy loadings, where the adsorption efficiency of HA was up to 10% higher. Samples with lower crystallinity and a more amorphous structure proved to be advantageous from a drug carrier point of view.

14) Following the drug loading experiments, drug delivery properties of the carriers were also investigated, *i.e.*, the release behavior was monitored in simulated fluids. Most of the systems exhibited the expected behavior, with drug release showing two distinct stages. An initial burst release was followed by a slower but sustained dissolution phase. The release of Doxy was examined and discussed from several perspectives.

a) The similar elemental composition and drug loading of the carriers allowed for a comparison between HA-based carriers and  $\beta$ -TCP carriers. Based on the dissolution profiles, it was clear that the initial release stage of carriers with similar chemical composition was significantly different. In comparison, a higher amount of released Doxy was measurable from apatite powders over the same time. HA and ion-doped HA showed more favorable drug release.

b) A negative correlation was observed between the amount of released active substance and the initial drug content, which was explained by Doxy-Doxy interactions.

c) The influencing parameters were mostly more significant in the case of lower drug content, so they were investigated in the following. Both Si and Mg played a role in decreasing of Doxy release rate. The retard effect of these carriers was visible, resulting in up to a 4% lower cumulative drug release percentage compared to unsubstituted carriers.

d) The morphology of the carrier proved to be a more dominant influencing factor than the chemical composition. Both the dissolution profiles and the results of drug release studies indicated that regular spherical morphology enabled a more uniform antibiotic release. In other words, Fickian diffusion can be achieved even with morphological modifications.

e) The regular morphology enhances the controllability of LDDS, which was confirmed by the gradual and continuous nature of the initial burst phase (in contrast to the behavior observed in the case of nanopowder carriers, where no initial jump was observed). A more uniform surface from an energetic point of view favored the formation of secondary interactions, the nature of which bonds influenced the release rate. This observation was further supported by the higher determination coefficient values.

f) Measurement of long-term release using the UV-VIS spectrophotometric method, in simulated body fluid (SBF), was not feasible due to the disturbance of the solution over time. Consequently, the samples were also examined in phosphate-buffered saline (PBS). The results of the 15-day measurements demonstrated that both HA and ion-doped HA carriers with regular spherical morphology were suitable for providing sustained Doxy release. Furthermore, the experiments also highlighted that the concentration of the dissolution medium in which the

given LDDS is tested has a significant influence on the release. PBS, with lower ion concentrations, led to more intensive Doxy diffusion.

Following this experimental section, the implementation of HA microspheres in implant coatings was carried out. Accordingly, the **sixth chapter** discussed the combination of metal implants and DDSs. The first part of the chapter focused on the preparation and optimization of porous PLA coatings. Doxy-containing coatings were produced based on the optimized parameters, and these coatings were investigated under *in vitro* conditions.

15) The dip-coating surface modification technique was suitable for the preparation of porous PLA coatings. The change in the porosity of the coating was examined as a function of solvent, concentration of the polymer solution, withdrawal speed, and immersion time.

a) The nature of the solvent, more precisely its boiling point, is a crucial parameter for the formation of open pores. Low-boiling-point solvents lead to the formation of smaller diameter pores.

b) Response Surface Methodology (RSM) was used to investigate the effects of PLA concentration, immersion time, and withdrawal speed on pore diameter and coating thickness. A Box-Behnken design matrix was selected to perform an efficient and rapid optimization study. The empirical relationships obtained here are valid only within the levels investigated.

i) The largest pore diameter and thickest coating can be achieved by maintaining the PLA solution concentration and withdrawal speed at their maximum levels while minimizing immersion time.

ii) The concentration of the dipping polymer solution played a decisive role in the spontaneous formation of micropores in the coating.

iii) The optimization method used proved to be adequate, as the properties of the coatings produced at the optimized parameters corresponded to the calculated values obtained during experimental design (the calculated average pore diameter was 2.7  $\mu\text{m}$ , while the experimentally determined average pore diameter based on SEM images was  $2.63\pm 0.55$   $\mu\text{m}$ ).

16) PLA-Doxy and PLA-HA-Doxy coatings, with different drug content, were prepared at the optimized parameters and studied.

a) The homogeneity of the coatings was supported by thermal analysis in addition to EDX mapping analysis. Coatings containing HA (as an additive) were found to be more advantageous thermally than pure PLA coatings. At the same time, the presence of HA microspheres increased the surface pore diameter (approximately 40% larger average pore diameter compared to pure PLA coatings).

b) Both the presence of the active substance and HA microspheres in the coating changed its wettability, enhancing the hydrophilic nature of the coatings. In this sense, both HA and the antibacterial agent confer better bioactivity to the coating.

c) Based on the electrochemical corrosion tests, it was established that the large pore size weakened the corrosion resistance. On the other hand, Doxy molecules improve the corrosion resistance of the PLA coating, thus serving not only as an active substance but also as a corrosion inhibitor. A positive correlation was observed between the drug content of the coating and its resistance to corrosion, which was confirmed by both PP and EIS tests. The thickness of the coating also plays a crucial role in reducing charge transfer processes.

17) The Doxy release from polymer-based coatings exhibited controlled and multi-step dissolution behavior in SBF. HA, in the case of coatings, was capable of forming secondary bonds and electrostatic attractions with Doxy molecules, resulting in reduced release rates. In other words, the addition of HA to PLA coatings can increase the release time of antibacterial agents.

18) The diffusion of Doxy from these coatings is a complex process, which was also supported by the release kinetics study. However, during the investigated period, the relaxation degree of the polymer chains had minimal impact on the release of drug molecules.

19) The constancy of the uniform and clearly defined release mechanism during the examined time proved the stability of the coatings.

In the seventh and **final chapter** of the doctoral thesis, the investigation of a new morphology Doxy carrier, namely polymer-based nanofibers, as local drug carriers was proposed. However, the novelty of the research presented in this part lies not only in the examined systems but also in the innovation of monitoring *in vitro* drug release using the differential-pulse voltammetry method. The following results were obtained during the experiment:

20) Using the electrospinning method, pure PLA and PLA nanofibers containing HA could be produced.

a) As supported by the SEM images, the use of a binary solvent mixture during the preparation of the starting polymer solution facilitated the formation of nanoscale fibers and it resulted in the development of a slightly rough surface morphology of the fibers.

b) The diameter distribution of the fibers and the average fiber diameter were a function of the chemical composition of the starting mixture. The additive (HA) caused a change in the physical properties of the polymeric mixture, leading to a significant decrease in the fiber diameter.

c) The point connections created between continuous fibers enabled the formation of porous structures, which advantageous 3D structures proved promising in dental applications.

21) The surface and spatial characteristics of the nanofibers allowed for the binding of Doxy to the fibers during the post-electrospinning process. The adsorption efficiency was on average between 70-80%, the process mainly depended on the concentration of the initial drug solution.

22) *In vitro* and *in situ* monitoring of drug release from carriers with such specific morphology and properties, was achievable through an electrochemical method.

a) The GC electrode proved to be suitable for determining the electrochemical fingerprint of Doxy molecules containing electrochemically active functional groups.

b) Under optimized conditions, the DPV method was adequate for real-time monitoring of Doxy release under *in vitro* conditions. The appropriate selection of the input parameters ensured the sufficient sensitivity of the method.

23) The release of Doxy from the nanofibers showed similar behavior as observed in previous parts of the thesis, where LDDSs based on carriers with different morphologies and material qualities were discussed. The negative correlation between the initial Doxy content of the fibers and the amount of released drug was demonstrated.

24) The burst release can be attributed to the rapid diffusion of weakly bound molecules, while achieving sustained release also depended on the presence of agglomerates of adsorbed drug molecules, alongside the diameter of the fibers.

25) The release kinetics showed behavior according to Korsmeyer-Peppas, regardless of the nature of the investigated system. The values of the diffusion exponent reflected the complexity of the systems through the not full Fick release.

26) Carriers with a fibrous morphology imitating the extracellular matrix were suitable for sustained drug release, which was supported by both electrochemical and spectrophotometric measurements. The DPV method was validated using conventional UV-VIS spectrophotometric investigations.

a) The applicability of the DPV method for measuring the release of Doxy from PLA and PLA-based nanofibers was confirmed by both model-independent and model-dependent approaches. The obtained release profiles met the similarity criterion in pairs.

b) This simple, rapid, efficient, and sufficiently sensitive method proved to be an alternative analytical procedure. The absence of sampling allows for the examination of the system without any external factors influencing the dissolution kinetics.

The research presented in the doctoral thesis highlights the key role of the carrier material properties in terms of the release of Doxy. The nature of the carrier, the appropriate material composition, and morphology enables to achieve controlled drug release. Through the investigation of the parameters influencing the release, the LDDS can be easily adapted to the therapeutic needs. These results contribute to the efficient design, development, production and *in vivo* application of these systems.

## References

- [1] D. Paolino *et al.*, *Drug delivery systems principles of controlled drug delivery*, Encyclopedia of Medical Devices and Instrumentation, Second Edition, John Wiley & Sons, Inc, **2016**, 437-495, doi: 10.1002/0471732877.emd274.
- [2] S. Adepu and S. Ramakrishna, *Controlled drug delivery systems: Current status and future directions*, *Molecules*, 26, 19, **2021**, doi: 10.3390/molecules26195905.
- [3] E. Güven, *Nanotechnology-based drug delivery systems in orthopedics*, *Jt. Dis. Relat. Surg.*, 32, 1, 267–273, **2021**, doi: 10.5606/ehc.2021.80360.
- [4] Z. A. B. Elneel Ahmed Mohamed, *Anxiety and Depression in a Sample of Disfigured Orofacial Cancer Patients at Khartoum Teaching Dental Hospital, Sudan*, *Journal of Advanced Medical and Dental Sciences Research*, 6, 2, 59–65, **2018**, doi: 10.21276/jamdsr.
- [5] J. V. Costa, J. Portugal, C. B. Neves, and A. F. Bettencourt, *Should local drug delivery systems be used in dentistry?*, *Drug Deliv. Transl. Res.*, 12, 6, 1395–1407, **2022**, doi: 10.1007/s13346-021-01053-x.
- [6] S. S. C A Squier, *Enhancing effect of chitosan on peptide drug delivery across buccal mucosa*, *Biomaterials*, 21, 20, 2067–71, **2000**, doi: 10.1016/s0142-9612(00)00134-4.
- [7] F. K. Silvana Papagerakis, *Controlled Drug Delivery Systems for Oral Cancer Treatment-Current Status and Future Perspectives*, 11, 7, 302, **2019**, doi: 10.3390/pharmaceutics11070302.
- [8] Michelle Franz-Montan, *Recent advances and perspectives in topical oral anesthesia*, *Expert Opinion on Drug Delivery*, 14, 5, 673–684, **2017**, doi: 10.1080/17425247.2016.1227784.
- [9] P. Chinavinijkul, K. Riansuwan, P. Kiratisin, S. Srisang, and N. Nasongkla, *Dip- and Spray-coating of Schanz pin with PLA and PLA nanosphere for prolonged antibacterial activity*, *J. Drug Deliv. Sci. Technol.*, 65, 102667, **2021**, doi: 10.1016/j.jddst.2021.102667.
- [10] K. Puri. and N Puri, *Local drug delivery agents as adjuncts to endodontic and periodontal therapy*, *J Med Life*, 6, 4, 414–9, **2013**.
- [11] D. T. de C. Andréa C dos Reis, *In vitro study of the antibacterial properties and impact strength of dental acrylic resins modified with a nanomaterial*, *J Prosthet Dent.*, 115, 2, 238–46, **2016**, doi: 10.1016/j.prosdent.2015.09.003.
- [12] Abtahi J, Agholme F, Sandberg O, Aspenberg P., *Effect of Local vs. Systemic Bisphosphonate Delivery on Dental Implant Fixation in a Model of Osteonecrosis of the Jaw*, *Journal of Dental Research*, 92, 3, **2012**, doi: 10.1177/0022034512472335.
- [13] Goodman SB, Yao Z, Keeney M, Yang F., *The future of biologic coatings for orthopaedic implants*, 34, 13, 3174–83, **2013**, doi: 10.1016/j.biomaterials.2013.01.074.
- [14] Wei Y, Deng Y, Ma S, Ran M, Jia Y, Meng J, Han F, Gou J, Yin T, He H, Wang Y, Zhang Y, Tang X., *Local drug delivery systems as therapeutic strategies against periodontitis: A systematic review*, *J Control Release*, 333, 10, 269–82, **2021**, doi: 10.1016/j.jconrel.2021.03.041.
- [15] S. K. Nandi *et al.*, *Understanding osteomyelitis and its treatment through local drug delivery system*, *Biotechnol. Adv.*, 34, 8, 1305–1317, **2016**, doi: 10.1016/j.biotechadv.2016.09.005.
- [16] F. Meng, Z. Yin, X. Ren, Z. Geng, and J. Su, *Construction of Local Drug Delivery System on Titanium-Based Implants to Improve Osseointegration*, *Pharmaceutics*, 14, 5, **2022**, doi: 10.3390/pharmaceutics14051069.
- [17] P. Bertsch, L. Schneider, G. Bovone, M. W. Tibbitt, P. Fischer, and S. Gstöhl, *Injectable biocompatible hydrogels from cellulose nanocrystals for locally targeted sustained drug release*, *ACS Appl. Mater. Interfaces*, 11, 42, 38578–38585, **2019**, doi: 10.1021/acsami.9b15896.
- [18] Rajeshwari H.R. *et al.*, *Local drug delivery systems in the management of periodontitis: A scientific review*, *J. Controlled Release*, 307, 393–409, **2019**, doi: 10.1016/j.jconrel.2019.06.038.
- [19] E. Feyzioğlu-Demir, Ö. B. Üzümlü, and S. Akgöl, *Swelling and diffusion behaviour of spherical morphological polymeric hydrogel membranes (SMPHMs) containing epoxy groups and their application as drug release systems*, *Polym. Bull.*, 80, 6, 6567–6590, **2023**, doi: 10.1007/s00289-022-04368-y.
- [20] M.L. Bruschi, *Main mechanisms to control the drug release*, in *Strategies to Modify the Drug Release from Pharmaceutical Systems*, Elsevier, **2015**, 37–62. doi: 10.1016/b978-0-08-100092-2.00004-7.

- [21] T. K. Giri, K. Kumar, A. Alexander, Ajazuddin, H. Badwaik, and D. K. Tripathi, *A novel and alternative approach to controlled release drug delivery system based on solid dispersion technique*, Bull. Fac. Pharm. Cairo Univ., 50, 2, 147–159, **2012**, doi: 10.1016/j.bfopcu.2012.07.002.
- [22] M. Seidenstuecker *et al.*, *Composite material consisting of microporous  $\beta$ -TCP ceramic and alginate for delayed release of antibiotics*, Acta Biomater., 51, 433–446, **2017**, doi: 10.1016/j.actbio.2017.01.045.
- [23] R. Detsch, J. Will, J. Hum, J. A. Roether, and A. R. Boccaccini, *Biomaterials in Cell culture technology*, Springer, Cham, **2018**, 91–105. doi: 10.1007/978-3-319-74854-2\_6.
- [24] G. Schmalz and D. Arenholt-Bindslev, *Biocompatibility of dental materials*. Springer Berlin, Heidelberg, **2009**. doi: 10.1007/978-3-540-77782-3.
- [25] E. T. J. Chong, J. W. Ng, and P. C. Lee, *Classification and Medical Applications of Biomaterials—A Mini Review*, BIO Integr., 4, 2, 54–61, **2023**, doi: 10.15212/bioi-2022-0009.
- [26] S. V. Dorozhkin, *Calcium orthophosphates as bioceramics: State of the Art*, J. Funct. Biomater., 1, 1, 22–107, **2010**, doi: 10.3390/jfb1010022.
- [27] M. Taherimehr, R. Bagheri, and M. Taherimehr, *In-vitro evaluation of thermoplastic starch/ beta-tricalcium phosphate nano-biocomposite in bone tissue engineering*, Ceram. Int., 47, 11, 15458–15463, **2021**, doi: 10.1016/j.ceramint.2021.02.111.
- [28] A. Fihri, C. Len, R. S. Varma, and A. Solhy, *Hydroxyapatite: A review of syntheses, structure and applications in heterogeneous catalysis*, Coord. Chem. Rev., 347, 48–76, **2017**, doi: 10.1016/j.ccr.2017.06.009.
- [29] S. B. H. Farid, *Osteoinduction, osteoconduction, and osseointegration in Bioceramics: For Materials Science and Engineering*, Elsevier, **2019**, 77–96. doi: 10.1016/B978-0-08-102233-7.00003-3.
- [30] A. Szcześ, L. Hołysz, and E. Chibowski, *Synthesis of hydroxyapatite for biomedical applications*, Adv. Colloid Interface Sci., 249, 321–330, **2017**, doi: 10.1016/j.cis.2017.04.007.
- [31] S. Mondal, S. V. Dorozhkin, and U. Pal, *Recent progress on fabrication and drug delivery applications of nanostructured hydroxyapatite*, WIREs Nanomedicine Nanobiotechnology, 10, 4, e1504, **2018**, doi: 10.1002/wnan.1504.
- [32] H. Huang, M. Du, J. Chen, S. Zhong, and J. Wang, *Preparation and characterization of abalone shells derived biological mesoporous hydroxyapatite microspheres for drug delivery*, Mater. Sci. Eng. C, 113, 110969, **2020**, doi: 10.1016/j.msec.2020.110969.
- [33] Y. Zhao, Y. Zhang, F. Ning, D. Guo, and Z. Xu, *Synthesis and cellular biocompatibility of two kinds of HAP with different nanocrystal morphology*, J. Biomed. Mater. Res. B Appl. Biomater., 83B, 1, 121–126, **2007**, doi: 10.1002/jbm.b.30774.
- [34] R. Singh, S. Gautam, B. Sharma, P. Jain, and K. D. Chauhan, *Biopolymers and their classifications in Biopolymers and their Industrial Applications*, Elsevier, **2021**, 21–44. doi: 10.1016/b978-0-12-819240-5.00002-x.
- [35] W. He and R. Benson, *Polymeric biomaterials in Applied plastics engineering handbook: processing*, Materials and Applications: Second Edition, Elsevier Inc., **2017**, 145–164. doi: 10.1016/B978-0-323-39040-8.00008-0.
- [36] B. Osi, M. Khoder, A. A. Al-Kinani, and R. G. Alany, *Pharmaceutical, biomedical and ophthalmic applications of biodegradable polymers (BDPs): literature and patent review*, Pharm. Dev. Technol., 27, 3, 341–356, **2022**, doi: 10.1080/10837450.2022.2055063.
- [37] R. M. Raj, N. Duraisamy, and V. Raj, *Drug loaded chitosan/aloe vera nanocomposite on Ti for orthopedic applications*, in *Materials Today: Proceedings*, Elsevier Ltd, **2021**, 1714–1719. doi: 10.1016/j.matpr.2020.10.772.
- [38] S. Liu *et al.*, *Controllable drug release behavior of polylactic acid (PLA) surgical suture coating with ciprofloxacin (CPFX)-polycaprolactone (PCL)/ polyglycolide (PGA)*, Polymers, 12, 2, **2020**, doi: 10.3390/polym12020288.
- [39] A. A. Volokhova *et al.*, *Controlled drug release from electrospun PCL non-woven scaffolds via multi-layering and e-beam treatment*, Mater. Today Commun., 26, **2021**, doi: 10.1016/j.mtcomm.2021.102134.

- [40] A. Pirmoradian, Y. Behshad, F. Sharifi, S. Alipour, L. Jiang, and M. Sabzi, *Development of antibiotic releasing electrospun nanofibrous mats based on gelatin*, *Materials Chemistry Horizons*, 2, 3, 185–193, **2023**, doi: 10.22128/mch.2023.689.1040.
- [41] A. Wilson, *The formation of dry, wet, spunlaid and other types of nonwovens in Applications of Nonwovens in Technical Textiles*, Elsevier, **2010**, 3–17. doi: 10.1533/9781845699741.1.3.
- [42] E. M. Elmowafy, M. Tiboni, and M. E. Soliman, *Biocompatibility, biodegradation and biomedical applications of poly(lactic acid)/poly(lactic-co-glycolic acid) micro and nanoparticles*, *J. Pharm. Investig.*, 49, 4, 347–380, **2019**, doi: 10.1007/s40005-019-00439-x.
- [43] A. A. Konta, M. García-Piña, and D. R. Serrano, *Personalised 3D printed medicines: Which techniques and polymers are more successful?*, *Bioengineering*, 4, 4, **2017**, doi: 10.3390/bioengineering4040079.
- [44] M. S. Singhvi, S. S. Zinjarde, and D. V. Gokhale, *Poly(lactic acid): synthesis and biomedical applications*, *J. Appl. Microbiol.*, 127, 6, 1612–1626, **2019**, doi: 10.1111/jam.14290.
- [45] V. DeStefano, S. Khan, and A. Tabada, *Applications of PLA in modern medicine*, *Eng. Regen.*, 1, 76–87, **2020**, doi: 10.1016/j.engreg.2020.08.002.
- [46] E. A. Bakr, M. Gaber, D. R. Saad, and N. Salahuddin, *Comparative study between two different morphological structures based on polylactic acid, nanocellulose and magnetite for co-delivery of flurouracil and curcumin*, *Int. J. Biol. Macromol.*, 230, **2023**, doi: 10.1016/j.ijbiomac.2023.123315.
- [47] M. Gaur, S. Maurya, M. S. Akhtar, and A. B. Yadav, *Synthesis and evaluation of BSA-loaded PLGA-chitosan composite nanoparticles for the protein-based drug delivery system*, *ACS Omega*, 8, 21, 18751–18759, **2023**, doi: 10.1021/acsomega.3c00738.
- [48] Y. Zhao, J. Xu, and S. Peng, *Synthesis and evaluation of TaC nanocrystalline coating with excellent wear resistance, corrosion resistance, and biocompatibility*, *Ceram. Int.*, 47, 14, 20032–20044, **2021**, doi: 10.1016/j.ceramint.2021.03.333.
- [49] M. Prodana, D. Ionita, A. B. Stoian, I. Demetrescu, G. V. Mihai, and M. Enăchescu, *The design and characterization of new chitosan, bioglass and ZnO-based coatings on Ti-Zr-Ta-Ag*, *Coatings*, 13, 3, **2023**, doi: 10.3390/coatings13030493.
- [50] A. Woźniak *et al.*, *The influence of plasma-sprayed coatings on surface properties and corrosion resistance of 316L stainless steel for possible implant application*, *Arch. Civ. Mech. Eng.*, 21, 4, 148, **2021**, doi: 10.1007/s43452-021-00297-1.
- [51] M. A. Hassan, Z. Zamri, R. Daud, N. Redzuan, and I. Sudin, *The effect of PLA/HA coating thickness on crack formation and corrosion performance in Advanced Materials and Engineering Technologies*, 162, A. Ismail, W. M. Dahalan, and A. Öchsner, Eds., in *Advanced Structured Materials*, 162., Cham: Springer International Publishing, **2022**, 47–53. doi: 10.1007/978-3-030-92964-0\_6.
- [52] B. Ambrozini, A. Carlos Guastaldi, R. Donizetti Herculano, M. Carlos Romeiro Miranda, and M. Jafelici Junior, *Sol-gel based calcium phosphates coating deposited on Co-Cr-Ni-Mo alloys modified by laser beam irradiation for cardiovascular devices*, *Mater. Today Proc.*, 14, 663–670, **2019**, doi: 10.1016/j.matpr.2019.02.004.
- [53] T. Xue *et al.*, *Surface modification techniques of titanium and its alloys to functionally optimize their biomedical properties: Thematic review*, *Front. Bioeng. Biotechnol.*, 8, **2020**, doi: 10.3389/fbioe.2020.603072.
- [54] A. Bandyopadhyay, F. Espana, V. K. Balla, S. Bose, Y. Ohgami, and N. M. Davies, *Influence of porosity on mechanical properties and in vivo response of Ti6Al4V implants*, *Acta Biomater.*, 6, 4, 1640–1648, **2010**, doi: 10.1016/j.actbio.2009.11.011.
- [55] K. A. Kravanja and M. Finšgar, *A review of techniques for the application of bioactive coatings on metal-based implants to achieve controlled release of active ingredients*, *Mater. Des.*, 217, **2022**, doi: 10.1016/j.matdes.2022.110653.
- [56] S. S. Sidhu, M. A. H. Gepreel, and M. Bahraminasab, *Advances in titanium bio-implants: Alloy design, surface engineering and manufacturing processes*, *J. Mater. Res.*, 37, 16, 2487–2490, **2022**, doi: 10.1557/s43578-022-00661-8.
- [57] J. Adhikari, P. Saha, and A. Sinha, *Surface modification of metallic bone implants-Polymer and polymer-assisted coating for bone in-growth in Fundamental Biomaterials: Metals*, Elsevier, **2018**, 299–321. doi: 10.1016/B978-0-08-102205-4.00014-3.

- [58] S. Akshaya, P. K. Rowlo, A. Dukle, and A. J. Nathanael, *Antibacterial coatings for titanium implants: Recent trends and future perspectives*, *Antibiotics*, 11, 12, **2022**, doi: 10.3390/antibiotics11121719.
- [59] G. A. Fielding, N. Sarkar, S. Vahabzadeh, and S. Bose, *Regulation of osteogenic markers at late stage of osteoblast differentiation in silicon and zinc doped porous TCP*, *J. Funct. Biomater.*, 10, 4, 48, **2019**, doi: 10.3390/jfb10040048.
- [60] D. D. S. Tavares, L. D. O. Castro, G. D. D. A. Soares, G. G. Alves, and J. M. Granjeiro, *Synthesis and cytotoxicity evaluation of granular magnesium substituted  $\beta$ -tricalcium phosphate*, *J. Appl. Oral Sci.*, 21, 1, 37–42, **2013**, doi: 10.1590/1678-7757201302138.
- [61] A. M. Brahim Chafik El Idrissi, *XRD and FTIR Analysis of magnesium substituted tricalcium calcium phosphate using a wet precipitation method*, *Biointerface Res. Appl. Chem.*, 11, 1, 8034-8042, **2021**, doi: 10.33263/BRIAC111.80348042.
- [62] K. Prem Ananth *et al.*, *Structural and chemical analysis of silica-doped  $\beta$ -TCP ceramic coatings on surgical grade 316L SS for possible biomedical application*, *J. Asian Ceram. Soc.*, 3, 3, 317–324, **2015**, doi: 10.1016/j.jascer.2015.06.004.
- [63] R. Barabás, N. I. Farkas, C. L. Nagy, O. Cadar, C. Moisa, and L. Bizo, *Adsorption and desorption behavior of natural and synthetic active compounds on hydroxyapatite-based nanocomposites*, *Ceram. Int.*, 47, 6, 8584–8592, **2021**, doi: 10.1016/j.ceramint.2020.11.226.
- [64] H. Baradari *et al.*, *Calcium phosphate porous pellets as drug delivery systems: Effect of drug carrier composition on drug loading and in vitro release*, *J. Eur. Ceram. Soc.*, 32, 11, 2679-2690, **2012**, doi: 10.1016/j.jeurceramsoc.2012.01.018.
- [65] H. Baradari, C. Damia, M. Dutreih-Colas, E. Champion, D. Chulia, and M. Viana,  *$\beta$ -TCP porous pellets as an orthopaedic drug delivery system: Ibuprofen/carrier physicochemical interactions*, *Sci. Technol. Adv. Mater.*, 12, 5, **2011**, doi: 10.1088/1468-6996/12/5/055008.
- [66] J. C. Colpo, C. Pigatto, N. Brizuela, J. Aragón, and L. A. L. dos Santos, *Antibiotic and anesthetic drug release from double-setting  $\alpha$ -TCP cements*, *J. Mater. Sci.*, 53, 10, 7112-7124, **2018**, doi: 10.1007/s10853-018-2071-4.
- [67] L. Marincas *et al.*, *Hydroxyapatite and silicon-modified hydroxyapatite as drug carriers for 4-aminopyridine*, *Crystals*, 11, 9, **2021**, doi: 10.3390/cryst11091124..
- [68] R. Barabas, M. Rigo, M. Sarkozi, M. A. Hoaghia, and O. Cadar, *Hydroxyapatite - Carbon nanotube composites for drug delivery applications*, *Braz. J. Chem. Eng.*, 36, 2, 913-922, **2019**, doi: 10.1590/0104-6632.20190362s20180181.
- [69] J. Lucas-Aparicio *et al.*, *Silicon-calcium phosphate ceramics and silicon-calcium phosphate cements: Substrates to customize the release of antibiotics according to the idiosyncrasies of the patient*, *Mater. Sci. Eng. C*, 106, 110173, **2020**, doi: 10.1016/j.msec.2019.110173.
- [70] C. Lindahl, W. Xia, J. Lausmaa, and H. Engqvist, *Incorporation of active ions into calcium phosphate coatings, their release behavior and mechanism*, *Biomed. Mater. Bristol*, 7, 4, **2012**, doi: 10.1088/1748-6041/7/4/045018.
- [71] S. A. Seyhan, D. B. Alkaya, S. Cesur, F. N. Oktar, and O. Gunduz, *Preparation and characterization of pure natural hydroxyapatite derived from seashells for controlled drug delivery*, *J. Aust. Ceram. Soc.*, **2022**, doi: 10.1007/s41779-022-00739-w.
- [72] A. R. Ahmady, K. Razmjooee, V. Nazar, and S. Saber-Samandari, *Alginate carrier as a controlled thymol delivery system: Effect of particle size*, *Mater. Chem. Phys.*, 294, **2023**, doi: 10.1016/j.matchemphys.2022.126982.
- [73] G. Zhu, R. Zhao, Y. Li, and R. Tang, *Multifunctional Gd,Ce,Tb co-doped  $\beta$ -tricalcium phosphate porous nanospheres for sustained drug release and bioimaging*, *J. Mater. Chem. B*, 4, 22, 3903-3910, **2016**, doi: 10.1039/c5tb02767e.
- [74] Ö. Yıldız, *Combined precipitation and spray drying for the synthesis of hydroxyapatite nanopowders as soft spherical granules*, *Ceram. Int.*, 44, 16, 19809–19817, **2018**, doi: 10.1016/j.ceramint.2018.07.238.
- [75] E. Skwarek, W. Janusz, and D. Sternik, *Adsorption of citrate ions on hydroxyapatite synthesized by various methods*, *J. Radioanal. Nucl. Chem.*, 299, 3, 2027–2036, **2014**, doi: 10.1007/s10967-013-2825-z.

- [76] N. I. Farkas *et al.*, *The effect of chemical composition and morphology on the drug delivery properties of hydroxyapatite-based biomaterials*, *Ceram. Int.*, 49, 15, 25156–25169, **2023**, doi: 10.1016/j.ceramint.2023.05.047.
- [77] E. S. Bogyá, M. Czíkó, G. Szabó, and R. Barabás, *The red beetroot extract antioxidant activity and adsorption kinetics onto hydroxyapatite-based materials*, *J. Iran. Chem. Soc.*, 10, 3, 491–503, **2013**, doi: 10.1007/s13738-012-0183-3.
- [78] M. Parent, H. Baradari, E. Champion, C. Damia, and M. Viana-Trecant, *Design of calcium phosphate ceramics for drug delivery applications in bone diseases: A review of the parameters affecting the loading and release of the therapeutic substance*, *J. Controlled Release*, 252, 1–17, **2017**, doi: 10.1016/j.jconrel.2017.02.012.
- [79] M. Mulazzi *et al.*, *Medicated Hydroxyapatite/Collagen Hybrid Scaffolds for Bone Regeneration and Local Antimicrobial Therapy to Prevent Bone Infections*, *Pharmaceutics*, 13, 7, 1090, **2021**, doi: 10.3390/pharmaceutics13071090.
- [80] Y. Wang, M. S. Hassan, P. Gunawan, R. Lau, X. Wang, and R. Xu, *Polyelectrolyte mediated formation of hydroxyapatite microspheres of controlled size and hierarchical structure*, *J. Colloid Interface Sci.*, 339, 1, 69–77, **2009**, doi: 10.1016/j.jcis.2009.07.023.
- [81] N. I. Farkas *et al.*, *Preparation and characterization of Doxycycline-loaded electrospun PLA/HAP nanofibers as a drug delivery system*, *Materials*, 15, 6, **2022**, doi: 10.3390/ma15062105.
- [82] S. Jose *et al.*, *Synthesis of luminescent Mg-incorporated hydroxyapatite by reflux condensation method: Photoluminescence, in-vitro drug release and kinetic studies*, *Mater. Today Proc.*, 58, 836–845, **2022**, doi: 10.1016/j.matpr.2021.09.390.
- [83] K. T. Arul *et al.*, *Novel multifunctional of magnesium ions (Mg<sup>++</sup>) incorporated calcium phosphate nanostructures*, *J. Alloys Compd.*, 730, 31–35, **2018**, doi: 10.1016/j.jallcom.2017.09.254.
- [84] M. U. Munir *et al.*, *Nano-hydroxyapatite as a delivery system: overview and advancements*, *Artif. Cells Nanomedicine Biotechnol.*, 49, 1, 717–727, **2021**, doi: 10.1080/21691401.2021.2016785.
- [85] T. Kokubo and S. Yamaguchi, *Simulated body fluid and the novel bioactive materials derived from it*, *J. Biomed. Mater. Res. A*, 107, 5, 968–977, **2019**, doi: 10.1002/jbm.a.36620.
- [86] B. Kundu *et al.*, *Development of new localized drug delivery system based on ceftriaxone-sulbactam composite drug impregnated porous hydroxyapatite: a systematic approach for in vitro and in vivo animal trial*, *Pharm. Res.*, 27, 8, 1659–1676, **2010**, doi: 10.1007/s11095-010-0166-y.
- [87] M.L. Bruschi, *Mathematical models of drug release in Strategies to Modify the Drug Release from Pharmaceutical Systems*, Elsevier, **2015**, 63–86. doi: 10.1016/b978-0-08-100092-2.00005-9.
- [88] F. Tamimi *et al.*, *Doxycycline sustained release from brushite cements for the treatment of periodontal diseases*, *J. Biomed. Mater. Res. A*, 85A, 3, 707–714, **2008**, doi: 10.1002/jbm.a.31610.
- [89] S. Tabassum *et al.*, *Efficient drug delivery system for bone repair by tuning the surface of hydroxyapatite particles*, *RSC Adv.*, 6, 107, 104969–104978, **2016**, doi: 10.1039/C6RA24551J.
- [90] N. A. Singh, A. K. A. Mandal, and Z. A. Khan, *Fabrication of PLA-PEG nanoparticles as delivery systems for improved stability and controlled release of Catechin*, *J. Nanomater.*, 2017, 1–9, **2017**, doi: 10.1155/2017/6907149.
- [91] O. C. Onder, M. A. Nazeer, E. Yilgör, and I. Yilgör, *Spontaneous formation of microporous poly(lactic acid) coatings*, *Prog. Org. Coat.*, 125, 249–256, **2018**, doi: 10.1016/j.porgcoat.2018.09.016
- [92] N. Argarate *et al.*, *Biodegradable Bi-layered coating on polymeric orthopaedic implants for controlled release of drugs*, *Mater. Lett.*, 132, 193–195, **2014**, doi: 10.1016/j.matlet.2014.06.070.
- [93] S. Sonjan, G. M. Ross, S. Mahasaranon, B. Sinkangam, S. Intanon, and S. Ross, *Biodegradable hydrophilic film of crosslinked PVA/silk sericin for seed coating: the effect of crosslinker loading and polymer concentration*, *J. Polym. Environ.*, 29, 1, 323–334, **2021**, doi: 10.1007/s10924-020-01867-9.

- [94] S. Buapool, N. Thavarungkul, N. Srisukhumbowornchai, and P. Termsuksawad, *Modeling and analysis of the effect of dip-spin coating process parameters on coating thickness using factorial design method*, *Adv. Mater. Sci. Eng.*, 2017, **2017**, doi: 10.1155/2017/9639306.
- [95] A. Zhang, H. Bai, and L. Li, *Breath figure: a nature-inspired preparation method for ordered porous films*, *Chem. Rev.*, 115, 18, 9801–9868, **2015**, doi: 10.1021/acs.chemrev.5b00069.
- [96] Ameenuzzafar *et al.*, *Improvement of ocular efficacy of levofloxacin by bioadhesive Chitosan coated PLGA nanoparticles: Box-behnken design, in-vitro characterization, antibacterial evaluation and scintigraphy study*, *Iran. J. Pharm. Res.*, 19, 1, 292–311, **2020**, doi: 10.22037/ijpr.2019.15318.13016.
- [97] B. Hou, Y. Liu, H. Chen, and Y. Yang, *In vitro bioactivity, bio-corrosion resistance and antibacterial property of laser cladded HA coatings with different content of ZnO on Ti-6Al-4V substrate*, *Mater. Res.*, 22, **2019**, doi: 10.1590/1980-5373-MR-2018-0744.
- [98] W. Zhang *et al.*, *Strengthened corrosion control of poly (lactic acid) (PLA) and poly ( $\epsilon$ -caprolactone) (PCL) polymer-coated magnesium by imbedded hydrophobic stearic acid (SA) thin layer*, *Corros. Sci.*, 112, 327–337, **2016**, doi: 10.1016/j.corsci.2016.07.027.
- [99] O. Yigit, B. Dikici, and N. Ozdemir, *Hydrothermal synthesis of nanocrystalline hydroxyapatite–graphene nanosheet on Ti-6Al-7Nb: mechanical and in vitro corrosion performance*, *J. Mater. Sci. Mater. Med.*, 32, 4, **2021**, doi: 10.1007/s10856-021-06514-w.
- [100] N. Cotelan, M. Rak, M. Bele, A. Cör, L. M. Muresan, and I. Milošev, *Sol-gel synthesis, characterization and properties of TiO<sub>2</sub> and Ag-TiO<sub>2</sub> coatings on titanium substrate*, *Surf. Coat. Technol.*, 307, 790–799, **2016**, doi: 10.1016/j.surfcoat.2016.09.082.
- [101] A. I. Rezk, H. M. Mousa, J. Lee, C. H. Park, and C. S. Kim, *Composite PCL/HA/simvastatin electrospun nanofiber coating on biodegradable Mg alloy for orthopedic implant application*, *J. Coat. Technol. Res.*, 16, 2, 477–489, **2019**, doi: 10.1007/s11998-018-0126-8.
- [102] S. K. Shukla and M. A. Quraishi, *The effects of pharmaceutically active compound doxycycline on the corrosion of mild steel in hydrochloric acid solution*, *Corros. Sci.*, 52, 2, 314–321, **2010**, doi: 10.1016/j.corsci.2009.09.017.
- [103] L. Y. Cui *et al.*, *Degradation mechanism of micro-arc oxidation coatings on biodegradable Mg-Ca alloys: The influence of porosity*, *J. Alloys Compd.*, 695, 2464–2476, **2017**, doi: 10.1016/j.jallcom.2016.11.146.
- [104] Alécio ABW, Ferreira CF, Babu J, Shokuhfar T, Jo S, Magini R, Garcia-Godoy F. *Doxycycline Release of Dental Implants With Nanotube Surface, Coated With Poly Lactic-Co-Glycolic Acid for Extended pH-controlled Drug Delivery*, *J Oral Implantol.*, 45, 4, 267–273, **2019**, doi: 10.1563/aaid-joi-D-18-00069.
- [105] E. D. de Avila *et al.*, *Anti-bacterial efficacy via drug-delivery system from layer-by-layer coating for percutaneous dental implant components*, *Appl. Surf. Sci.*, 488, 194–204, **2019**, doi: 10.1016/j.apsusc.2019.05.154.
- [106] Z. Assadi, G. Emtiazi, and A. Zarrabi, *Hyperbranched polyglycerol coated on copper oxide nanoparticles as a novel core-shell nano-carrier hydrophilic drug delivery model*, *J. Mol. Liq.*, 250, 375–380, **2018**, doi: 10.1016/j.molliq.2017.12.031.
- [107] N. Mederle *et al.*, *Innovative biomaterials based on collagen-hydroxyapatite and doxycycline for bone regeneration*, *Adv. Mater. Sci. Eng.*, 2016, 1–5, **2016**, doi: 10.1155/2016/3452171.
- [108] X. Wang *et al.*, *Poly(lactide-co-glycolide) encapsulated hydroxyapatite microspheres for sustained release of doxycycline*, *Mater. Sci. Eng. B*, 177, 4, 367–372, **2012**, doi: 10.1016/j.mseb.2011.12.030.
- [109] I. J. Macha, S. Cazalbou, B. Ben-Nissan, K. L. Harvey, and B. Milthorpe, *Marine structure derived calcium phosphate-polymer biocomposites for local antibiotic delivery*, *Mar. Drugs*, 13, 1, 666–680, **2015**, doi: 10.3390/md13010666.
- [110] D. Lawrencja *et al.*, *Controlled release fertilizers: A review on coating materials and mechanism of release*, *Plants*, 10, 2, 1–26, **2021**, doi: 10.3390/plants10020238.
- [111] R. Cánovas, N. Slegers, A. L. N. Van Nuijs, and K. De Wael, *Tetracycline antibiotics: elucidating the electrochemical fingerprint and oxidation pathway*, *Chemosensors*, 9, 7, 187, **2021**, doi: 10.3390/chemosensors9070187.

- [112] N. I. Farkas, L. Marincaş, L. Barbu-Tudoran, R. Barabás, and G. L. Turdean, *Investigation of the Real-Time Release of Doxycycline from PLA-Based Nanofibers*, *J. Funct. Biomater.*, 14, 6, **2023**, doi: 10.3390/jfb14060331.
- [113] M. Ghorbani, F. Mahmoodzadeh, L. Yavari Maroufi, and P. Nezhad-Mokhtari, *Electrospun tetracycline hydrochloride loaded zein/gum tragacanth/poly lactic acid nanofibers for biomedical application*, *Int. J. Biol. Macromol.*, 165, 1312–1322, **2020**, doi: 10.1016/j.ijbiomac.2020.09.225.
- [114] C. R. Reshmi, S. V. Nair, and D. Menon, *From nonwoven fibers to woven nanotextiles: Electrospinning in drug delivery in Biomedical Applications of Electrospinning and Electrospinning*, Elsevier, **2021**, 123–156. doi: 10.1016/B978-0-12-822476-2.00003-0.
- [115] S. C. Chen, X. B. Huang, X. M. Cai, J. Lu, J. Yuan, and J. Shen, *The influence of fiber diameter of electrospun poly(lactic acid) on drug delivery*, *Fibers Polym.*, 13, 9, 1120–1125, **2012**, doi: 10.1007/s12221-012-1120-x.
- [116] I. Rus *et al.*, *Simple and fast analytical method for the evaluation of the encapsulation and release profile of doxorubicin from drug delivery systems*, *Farmacia*, 69, 4, 670–681, **2021**, doi: 10.31925/farmacia.2021.4.6.
- [117] A. I. Rezk, D. P. Bhattarai, J. Park, C. H. Park, and C. S. Kim, *Polyaniline-coated titanium oxide nanoparticles and simvastatin-loaded poly( $\epsilon$ -caprolactone) composite nanofibers scaffold for bone tissue regeneration application*, *Colloids Surf. B Biointerfaces*, 192, 111007, **2020**, doi: 10.1016/j.colsurfb.2020.111007